Strongly interacting WW system: Gold-plated modes

J. Bagger,[1] V. Barger,[2] K. Cheung,[3] J. Gunion,[4] T. Han,[5,4] G. A. Ladinsky,[6] R. Rosenfeld,[7] and C.-P. Yuan[6]

[1]*Department of Physics and Astronomy, The Johns Hopkins University, Baltimore, Maryland 21218*
[2]*Department of Physics, University of Wisconsin, Madison, Wisconsin 53706*
[3]*Department of Physics, Northwestern University, Evanston, Illinois 60208*
[4]*Davis Institute for High Energy Physics, Department of Physics, University of California at Davis, Davis, California 95616*
[5]*Fermi National Accelerator Laboratory, P.O. Box 500, Batavia, Illinois 60510*
[6]*Department of Physics and Astronomy, Michigan State University, East Lansing, Michigan 48824*
[7]*Department of Physics, Northeastern University, Boston, Massachusetts 02115*
(Received 16 June 1993)

In this paper we survey the signals and backgrounds for a strongly interacting electroweak symmetry-breaking sector at hadron supercolliders in the TeV region. We study the process $pp \to WWX$, and compute the rates for the "gold-plated" channels, where $W^\pm \to l^\pm \nu$ and $Z \to l^+ l^-$ ($l = e, \mu$), for a wide variety of models. Using a forward jet-tag, a central jet-veto, and a back-to-back lepton cut to suppress the standard model backgrounds, we demonstrate that the SSC and CERN LHC have substantial sensitivity to strong interactions in the electroweak symmetry-breaking sector.

PACS number(s): 12.60.$-$Fr, 13.38.Be, 13.38.Dg, 14.80.Bn

I. INTRODUCTION

During the past decade, the discovery of the W and Z bosons demonstrated that the gauge structure of the standard model (SM) is correct. However, little is known about the mechanism that gives the vector bosons their mass. In the standard model, they acquire mass because a scalar field, the Higgs doublet, has a nonzero vacuum expectation value v. At present, however, there is no experimental evidence in favor of the Higgs particle: all the precision measurements can be described by a Higgs-boson-free standard model.

Of course, the standard model without a Higgs boson cannot be a fundamental theory [1,2]. It is only an effective theory, breaking down below a few TeV. New physics must emerge below this scale, which the next round of accelerators had better be prepared to find.

WW scattering provides a particularly promising avenue for investigating this new physics (here and henceforth W generically denotes the W or Z boson, unless specified otherwise). The $WW \to WW$ cross section without a light Higgs boson violates perturbative unitarity at about 1 TeV. Consequently, new physics must couple to this channel in just such a way as to cure its bad high-energy behavior.

In this paper we will investigate signals and backgrounds for the process $pp \to WWX$ at hadron supercolliders, such as the Superconducting Super Collider (SSC) and CERN Large Hadron Collider (LHC). We will concentrate on the situation in which there are no new particles below 1 TeV. We shall study a variety of possible models, all of which are perfectly consistent with the data to date.

Of course, in such studies one must decide what is the "signal" and what is the "background." We will take the

signal to be the process $pp \to W_L W_L X$, as shown in Fig. 1, where L refers to longitudinal polarization (while the transverse polarization will be denoted by T). This definition of the signal is appropriate because the $W_L W_L$ channels couple most strongly for new physics, and $W_L W_L$ production is negligible unless the interactions among the W's are strong. Since we are mainly interested in physics for the electroweak symmetry-breaking sector, we will not include the contributions to our $W_L W_L$ signal from Yukawa couplings, such as $t\bar{t}H$ in the SM. The most difficult *background* to the $W_L W_L$ final state is $W_L W_T$ and $W_T W_T$ production: $pp \to W_L W_T X$ and $pp \to W_T W_T X$. Such processes are a background in the sense that their cross sections are essentially independent of strong interactions in the W sector; i.e., they are insensitive to new physics. Further, this background is irreducible in that the final state contains two real W's analogous to the signal of interest (ignoring polarization).

Ultimately, after appropriate cuts, the $W_L W_T + W_T W_T$ background is dominated by the "electroweak" (EW) diagrams, as shown in Fig. 2(a), which includes $W_T W_T$, $W_L W_T$ scattering diagrams and those in which W's are radiated or emitted via electroweak interactions. An additional contribution to the $W_T W_L + W_T W_T$ back-
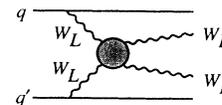

FIG. 1. Symbolic diagrams for the $W_L W_L \to W_L W_L$ scattering signal. The black region represents the $W_L W_L$ strongly interacting physics.
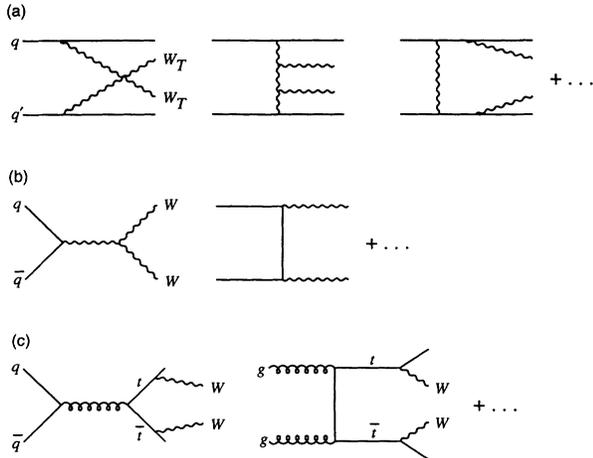
FIG. 2. Representative diagrams for backgrounds to the $W_L W_L$ signal: (a) EW processes; (b) lowest-order QCD processes, with possible additional QCD-jet radiation; and (c) top quark backgrounds.

ground arises from the $q\bar{q}$ annihilation processes illustrated in Fig. 2(b). Since both of these backgrounds are essentially independent of the new physics in the $W_L W_L$ channel, we are free to compute them using the standard model with a light (100-GeV) Higgs boson, for which $W_L W_L$ production is negligible. The difference between this computation and a first-principles computation of the background in a model which incorporates strong interactions in the $W_L W_L$ sector is negligible at the energies we consider. Finally, there are heavy-quark backgrounds, especially those associated with top-quark production and decay [Fig. 2(c)]. These too may be reliably computed in the SM once the top-quark mass is known.

For most of our signal estimates, we will simplify our calculations by using the Goldstone-boson equivalence theorem [1-3], which states that, at high energies, the external longitudinal vector bosons can be replaced by their corresponding would-be Goldstone bosons. This is both a computational and conceptual simplification, for it allows us to draw on our considerable experience with Goldstone-boson scattering in QCD. We will also use the effective W approximation [4,5] to connect the $W_L W_L$ subprocesses to the pp initial state.

We focus our attention on the "gold-plated" events, where the W and Z decay to charged leptonic final states ($l = e, \mu$). For the purpose of this study, we ignore final states where the bosons decay hadronically, as well as final states where either of the Z's decays into neutrinos. These final states should also be studied and will possibly improve the observability of electroweak symmetry breaking at the SSC and/or LHC [6].

Because we focus on the gold-plated leptonic channels, the only backgrounds to the $W_L W_L$ signal that we need to consider are those in which real $W_L W_T$ and $W_T W_T$ pairs are produced. As already noted, in the final analysis, the diagrams in Fig. 2(a) yield the most difficult backgrounds. We suppress these backgrounds by imposing further restrictions on the events. However, we must also deal with the additional background processes of

Figs. 2(b) and 2(c). The continuum pair production processes of Fig. 2(b) arising from $q\bar{q}$ annihilation (which we term the QCD background) contribute to the $W^+ W^-$, $W^\pm Z$, and ZZ channels. At lowest order, these annihilation processes have a very different final-state structure than the WW scattering processes of interest, where spectator quark jets are left behind when the incoming quarks radiate the initial-state W's that then scatter (see Fig. 1). Thus, even allowing for higher-order radiative corrections, the QCD background can be greatly suppressed by requiring a tagged forward jet. The heavy top-quark processes of Fig. 2(c), arising from $t\bar{t}$, $t\bar{t}W$, and $t\bar{t}Z$ production followed by t and $\bar{t}$ decays to real W's, contribute to the $W^+ W^-, W^\pm Z$, and $W^\pm W^\pm$ channels. Fortunately, these top-quark background processes have substantial jet activity at moderate rapidity and can be efficiently suppressed by requiring a central jet veto.

Indeed, it turns out that both the forward jet tag and the central jet veto are effective in reducing the backgrounds from the irreducible $LT + TT$ electroweak backgrounds as well. Nonetheless, if only jet tagging and/or vetoing is applied, a substantial EW $LT + TT$ background remains in the $W^\pm W^\pm$ and $W^+ W^-$ channels. This background remnant can be greatly reduced with little impact on the LL signal by requiring energetic leptons at low rapidity and, especially, requiring that the two leptons appearing in the final state be very back to back.

Because we use the effective W approximation for our signal, we can only estimate the effects of the tag and veto cuts. We use the exact standard model calculation with a 1-TeV Higgs boson to derive efficiencies for these cuts. Since these efficiencies should be relatively model independent, we can apply them to the effective W calculations to estimate the rate for each signal. The efficiency for the lepton cuts, including the back-to-back requirements if imposed, is obtained by employing the effective W approximation and decaying the final W's appropriately. The accuracy of this procedure was tested in the SM 1-TeV Higgs case. Good agreement was found between the lepton cut efficiencies obtained in the exact calculation and in the effective W calculation.

In Sec. II of this paper we study these procedures for the standard model. We take the signal to be a 1-TeV Higgs resonance and the electroweak background to be the SM rate for a light Higgs boson (we employ $m_H = 100$ GeV). We present the cuts that maximize the signal/background ratio while preserving a reasonable rate. We use the exact calculation to compute efficiencies for the forward jet tag and the central jet veto. In Sec. III we present the different models we will employ. We examine resonant and nonresonant scenarios, and frame our discussion in the language of chiral Lagrangians. In Sec. IV we examine the accuracy of our procedure in which we apply the cut efficiencies obtained from the exact SM calculation of Sec. II to the cross sections obtained using the equivalence theorem and the effective W approximation. We then present our basic numerical results and assess the reach of the SSC and LHC for each of the strongly interacting W-system models. Section V contains further discussion and comments. We conclude with some brief remarks in Sec. VI.

II. STANDARD MODEL

In this section, we discuss WW scattering in the standard model with a 1-TeV Higgs particle. Although it is argued [7] that the SM is not a consistent effective theory if $m_H \gtrsim 800$ GeV or so, we take this case as a prototype for models with strong WW scattering. We present the signal and background, calculated using the exact, order-α^2, matrix elements for $pp \to WWX$. We use these results to derive efficiencies for the forward jet tag and the central jet veto. The comparison of signal results to those found using the equivalence theorem and the effective W approximation will be presented in Secs. IV and V.

In this study we concentrate on the purely leptonic decay modes of the final-state W's, namely, the "gold-plated" events, with $W^\pm \to l^\pm \nu_l$ and $Z \to l^+ l^-$ ($l = e, \mu$). The experimental signature is given by two or more isolated, charged leptons in the central rapidity $[y(l)]$ region, with large transverse momenta (p_T). Although clean, these gold-plated channels carry the price of relatively small branching fractions for the purely leptonic W decays.

The diagram for longitudinal vector boson scattering is given symbolically in Fig. 1:

$$qq \to qq W_L W_L \ , \tag{2.1}$$

where W_L denotes a longitudinally polarized vector boson ($W_L \equiv W_L^\pm, Z_L$). If the interactions between W_L bosons are strong at high energies, we expect $W_L W_L$ scattering to be enhanced at large invariant mass. It is this enhancement which defines the signal we wish to isolate.

The irreducible backgrounds are shown in Fig. 2. At least one of the final W's produced in the background processes is transversely polarized. In particular, the cross sections for WW scattering to produce $W_L W_T$ or $W_T W_T$ pairs are essentially independent of the Higgs boson mass in the SM and are part of the background by definition. Other backgrounds include gluon exchange between quarks with initial- and final-state emission of two W's (both of which are dominantly transversely polarized) [8], and a variety of electroweak processes in which a final W_T arises via bremsstrahlung or emission from a primary quark or electroweak boson line. Continuum WW pair production arising from $q\bar{q}$ annihilation and gg fusion also contributes to the background. For cases with a $W^\pm$ in the final state, there is an especially important *reducible* background from heavy-quark production and decay.

It is important to note that two spectator quarks always emerge in association with the $W_L W_L$ scattering signal, but that spectators emerge in only a subset of the irreducible backgrounds. The spectator quarks usually appear in forward and/or backward regions, and have an energy of order 1 TeV and a p_T of order $M_W/2$. It is therefore possible to improve the signal-background ratio by tagging those quark jets (in particular, continuum pair production processes do not have a spectator quark jet at lowest order in perturbation theory) [9]. While studies have shown that tagging *two* high-p_T spectator jets substantially enhances the signal-background ratio, such double tagging proves to be too costly to the signal [10–13]. It has been recently suggested that tagging just one of these quarks as a single *energetic* jet can be just as efficient in suppressing the backgrounds that do not intrinsically require spectator jets, and far more efficient in retaining the signal for a heavy Higgs boson [13–15]. Thus, to isolate the heavy Higgs boson and other types of strong $W_L W_L$ signals, we will apply such a forward jet tag for most final-state channels [13–17].

The detailed characteristics of W_L emission and the associated spectator jets also play a role in separating $W_L W_L$ scattering from the background processes which *do* yield spectator jets (as well as two W's) in the final state. The crucial point to note is that the initial W_L's participating in the $W_L W_L$ scattering have a $1/(p_T^2 + M_W^2)^2$ distribution with respect to the quarks from which they are emitted. This is to be contrasted, for instance, with $W_T W_T$ scattering where the initiating W_T's have a $p_T^2/(p_T^2 + M_W^2)^2$ distribution with respect to the emitting quarks. The softer p_T distribution in the $W_L W_L$ case has two primary consequences. First, the final $W_L W_L$ pair is likely to have much more limited net transverse motion than $W_L W_T$ and $W_T W_T$ pairs produced through the various irreducible backgrounds. Second, the spectator quarks left behind tend to emerge with smaller p_T (order of $M_W/2$), and correspondingly larger rapidity, than those associated with the background processes containing spectator jets and $W_L W_T$ or $W_T W_T$ pairs.

There are several crucial secondary consequences resulting from the above special characteristics of $W_L W_L$ scattering. First, as discussed above, the jets from the gluon-exchange background and the electroweak background are generally harder and more central than those from the signal [12,16]. Therefore we will normally veto hard central jets to enhance the signal-background ratio [12,16,17]. Such a veto retains most of the signal events. As a further bonus, a central jet veto is especially effective in suppressing the reducible background from heavy-quark production and decay. The jets associated with this latter type of background populate a much more central region than do those from spectator quarks. Another consequence of the small p_T of the $W_L W_L$ system is that we expect the charged leptons from the decays of the two final W_L's to be very back to back in the transverse plane [16,17]. This is due not only to the limited p_T of the $W_L W_L$ system, but also to the fact that the bulk of the leptons emitted from each final W_L will have a significant (and relatively similar) fraction of the W_L's total momentum. The latter fact also implies that the leptons will generally be very energetic. A cut requiring that the leptons appearing in the final state be very energetic and very back to back will substantially reduce all backgrounds, while being highly efficient in retaining the $W_L W_L$ signal events.

We have already noted that the charged leptons will be required to be isolated. In order to completely eliminate the background from heavy quark production and decay

(say, b or c semileptonic decays) in all channels, we implicitly assume that it will be possible to implement an isolation requirement according to which the hadronic energy deposit within a cone $\Delta R < 0.3$ around the lepton must be less than about 5 GeV [18].

Before proceeding, we wish to reemphasize the precise definition of the signal and background that we employ. The results in this section will all be based on the full matrix-element calculations for the standard model. We define the heavy Higgs boson signal to be the difference between the cross section with a heavy Higgs boson and the result with a light Higgs boson: for example,

σ(signal for a 1-TeV Higgs boson)

$$=\sigma(m_H=1 \text{ TeV})-\sigma(m_H=100 \text{ GeV}) , \quad (2.2)$$

where all W helicities have been included for both m_H values. At SSC energies, the EW rate for production of W pairs in which one or both of the W's is transversely polarized is essentially independent of the Higgs boson mass, while $W_L W_L$ production is extremely small at $m_H = 100$ GeV. Thus the prescription (2.2) measures the production rate of longitudinally polarized W bosons at large m_H. We will sometimes refer to this definition of the signal as the "subtraction" result.

As stated earlier in the Introduction, we are only interested in the EW symmetry-breaking sector; we do not include contributions to the $W_L W_L$ final state arising from processes such as $gg, q\bar{q} \to t\bar{t}H$ and $gg \to H$ (via a top-quark loop) that depend upon the Yukawa couplings of the Higgs boson.

We now turn to a detailed discussion of the signals and backgrounds for the leptonic decay modes associated with each of the possible $W_L W_L$ scattering channels.

A. $W^+ W^- \to ZZ$, $ZZ \to ZZ$

We first consider the "gold-plated" events with four charged leptons from ZZ decays. This gives a clean and distinct signal because the ZZ pairs can be fully reconstructed. The disadvantage is the rather small leptonic branching fraction $B(ZZ \to 4l)=0.45\%$.

The major standard model backgrounds for this process arise from continuum ZZ production via tree-level processes at $O(\alpha^2)$, $O(\alpha^2 \alpha_s)$, and $O(\alpha^2 \alpha_s^2)$ [19–21]: for example,

$$qq \to ZZ + \text{jets} , \quad (2.3)$$

which we will refer to as the QCD background. This set of backgrounds includes, in particular, diagrams at order $\alpha^2 \alpha_s^2$ from gluon-exchange diagrams in which two quarks scatter via gluon exchange while two vector bosons are emitted from either the initial or final quark lines. Since the Z's are relatively weakly coupled to quark lines, this type of background is small in this case. At supercollider energies, the one-loop process

$$gg \to ZZ \quad (2.4)$$

is also not negligible. The total production rate is 30–70 % as large as that from $q\bar{q} \to ZZ$, depending on the top-quark mass [22]. However, we are interested in

the large $M(ZZ)$ region and require a very energetic jet in the final state; so the effective gluon luminosity is suppressed to a level where we can ignore gluon fusion in our calculations.

The $O(\alpha^4)$ electroweak production of transversely polarized Z pairs is another irreducible background [11,13,23]. Although it is formally higher order than Eq. (2.3) in terms of the electroweak coupling constant, the kinematics are so similar to the signal that it must also be included. We will refer to this as the electroweak (EW) background.

In a recent study, kinematical cuts were developed to suppress these backgrounds for detecting a heavy SM Higgs boson at the SSC and LHC [13]. We will use the same cuts:

$$p_T(l) > 40 \text{ GeV}, \quad |y(l)| < 2.5 , \quad (2.5)$$

$$M(ZZ) > 500 \text{ GeV}, \quad p_T(Z) > \tfrac{1}{4}\sqrt{M(ZZ)^2 - 4M_Z^2} ,$$

where $y(l)$ is the rapidity of the lepton l and $M(ZZ)$ is the invariant mass of the two Z's in the final state. The transverse momentum cut on the Z's is motivated by its facility in removing the QCD background [24]. As discussed above, a forward (or backward) jet tag is very effective in suppressing the QCD and EW backgrounds [13]. Therefore we will also require a tagged jet in the region

$$E(j_{\text{tag}}) > 1.0 \text{ (0.8) TeV} ,$$
$$3 < |y(j_{\text{tag}})| < 5, \quad p_T(j_{\text{tag}}) > 40 \text{ GeV} , \quad (2.6)$$

where the number outside (inside) the parentheses refers to the cut applied at the SSC (LHC).

The jet-tagging efficiency is about 60% for the signal. The combined cuts essentially eliminate the QCD background and substantially suppress the EW background. An additional cut requiring the leptons from opposite Z's to be back to back is not needed in this case.

B. $W^+ W^- \to W^+ W^-$, $ZZ \to W^+ W^-$

We next consider $W^+ W^-$ events in the $l \nu_l \bar{l} \nu_l$ final state, where $l = e, \mu$. The leptonic branching function is $B(WW \to l \bar{\nu}_l \bar{l} \nu_l)=4.7\%$, and so we expect a larger number of events in this channel. Although the two W's cannot be fully reconstructed, any s-channel resonance, such as the standard model Higgs boson, significantly enhances the production rate, and the $M(ll)$ spectrum peaks broadly at about one-half the resonance mass [14].

Unfortunately, there are now reducible backgrounds in addition to the irreducible backgrounds from continuum QCD and EW processes. The most important ones are

$$q\bar{q}, gg \to t\bar{t}, \quad gg \to t\bar{t}g, \quad qg \to t\bar{t}q, \quad q\bar{q} \to t\bar{t}g , \quad (2.7)$$

where the top quarks decay into real W's [25–27].

To reduce the backgrounds, we first impose stringent leptonic cuts

$p_T(l) > 100$ GeV, $|y(l)| < 2$,

$$\Delta p_T(ll) \equiv |\mathbf{p}_T(l_1) - \mathbf{p}_T(l_2)| > 450 \text{ GeV} , \quad (2.8)$$

$M(ll) > 250$ GeV, $\cos\phi_{ll} < -0.8$,

where $\Delta p_T(ll)$ and $\cos\phi_{ll}$ are, respectively, the difference of the transverse momenta and the cosine of the opening angle in the transverse plane of the two charged leptons. The cuts on these two variables are based on our earlier observations that the lepton-pair decay products are more energetic and more back to back in the transverse plane for signal events than for the backgrounds [16]. For example, the transverse momentum of the charged leptons, $p_T(l)$, for the signal will typically be of order $m_H/4$. For a 1-TeV Higgs boson, $\Delta p_T(ll) \sim m_H/2 = 500$ GeV.

We also impose the jet-tagging conditions [14]

$E(j_{\text{tag}}) > 1.5$ (1.0) TeV ,

$$3 < |y(j_{\text{tag}})| < 5, \quad p_T(j_{\text{tag}}) > 40 \text{ GeV} . \quad (2.9)$$

The $E(j_{\text{tag}})$ cut has been made slightly more stringent than Eq. (2.6) in order to control the much larger $t\bar{t}g$ background. We further suppress the top background by a central jet veto in which events with jets with [14]

$$p_T(j_{\text{veto}}) > 30 \text{ GeV}, \quad |y(j_{\text{veto}})| < 3 \quad (2.10)$$

are rejected. In Ref. [29], a central jet threshold of 25 GeV was used by the Solenoidal Detector Collaboration (SDC). Our choice in Eq. (2.10) is slightly more conservative. Vetoing is imposed at the primordial quark-gluon level in our computations. Additional (higher-order) QCD radiation is not included here.

Combining the cuts of Eqs. (2.8)–(2.10), we can reduce the backgrounds below the $W_L^+ W_L^-$ signal. Especially significant is the effective reduction of the large $t\bar{t}$ background. With the leptonic cuts of Eq. (2.8) imposed, the overall efficiency for jet tagging and vetoing is about 38% for the signal. We have chosen $m_t = 140$ GeV as representative in our background analyses throughout this paper. If the top quark is heavier, our jet-veto cut would be more effective and the $t\bar{t}j$ background would be easier to separate [14].

C. $W^+Z \rightarrow W^+Z$

We now turn to the WZ events with $l\bar{\nu}_l l\bar{l}$ final states. The leptonic branching fraction is $B(W^+Z \rightarrow l\bar{\nu}_l l\bar{l}) = 1.5\%$.

For this channel, we choose the leptonic acceptance cuts as follows:

$p_T(l) > 40$ GeV, $|y(l)| < 2.5$,

$$\not{p}_T > 75 \text{ GeV}, \quad M_T > 500 \text{ GeV}, \quad p_T(Z) > \tfrac{1}{4}M_T , \quad (2.11)$$

where $\not{p}_T$ denotes the missing transverse momentum and M_T is the cluster transverse mass of the WZ system, defined by [28]

$$M_T^2 = [\sqrt{M^2(lll) + p_T^2(lll)} + |\not{p}_T|]^2$$
$$- [\mathbf{p}_T(lll) + \not{p}_T]^2 . \quad (2.12)$$

Analogous to the cut on $p_T(Z)$ given in Eq. (2.5), the $p_T(Z)$ cut in Eq. (2.11) is useful for removing the QCD background.

To reduce the QCD and EW backgrounds, following Ref. [15], we tag a jet with

$E(j_{\text{tag}}) > 2.0$ (1.5) TeV ,

$$3 < |y(j_{\text{tag}})| < 5, \quad p_T(j_{\text{tag}}) > 40 \text{ GeV} . \quad (2.13)$$

We can reduce the background from Z and top-quark associated production;

$$q\bar{q}, gg \rightarrow Zt\bar{t} , \quad (2.14)$$

by imposing the jet vetoing of Eq. (2.10), with a looser cut $p_T(j_{\text{veto}}) > 60$ GeV.

The tagging plus vetoing efficiency is about 40% for the signal. As for the fully reconstructable $ZZ \rightarrow 4l$ mode, a back-to-back lepton cut is not needed here.

D. $W^+W^+ \rightarrow W^+W^+$

Finally, we discuss the like-sign W process with two like-sign charged leptons in the final state [30,12,16,31,17]. This mode is attractive because of the distinctive final state and absence of an order α^2 continuum background.

However, backgrounds to the $W_L^+ W_L^+$ signal do exist. In addition to the transversely polarized background from EW processes, there is the previously mentioned background contributing at order $\alpha^2\alpha_s^2$,

$$qq \rightarrow qqW^+W^+ , \quad (2.15)$$

in which a gluon is exchanged between the scattering quarks [8,32]. Since there is no lowest-order (α^2 or $\alpha^2\alpha_s$) background, this process is potentially significant for this channel. Finally, there is a background from associated $Wt\bar{t}$ production [12]:

$$q'\bar{q} \rightarrow Wt\bar{t} , \quad (2.16)$$

with $t \rightarrow W^+b$.

We first impose the leptonic cuts of Eq. (2.8), with the exception of a weaker cut $\Delta p_T(ll) > 200$ GeV. The back-to-back cuts are advantageous in the present channel [16,17]. We also apply the jet vetoing of Eq. (2.10) to this case, with a looser cut $p_T(j_{\text{veto}}) > 60$ GeV [12], and find that it greatly reduces the backgrounds.

Another potentially large background is that from $t\bar{t}$ production with a cascade decay, $\bar{t} \rightarrow \bar{b}W^- \rightarrow l^+X$. However, the l^+ from the $\bar{b}$ semileptonic decay is usually not isolated. When the l^+ is fast, the other hadrons from the $\bar{b}$ decay tend to be collinear with the l^+. We have not explicitly imposed a lepton isolation cut. Experimentally observable leptons are typically required to be isolated in a cone of size $\Delta R < 0.4$ in the rapidity–azimuthal-angle plane. Such an isolation requirement would have negligible impact on the signal and backgrounds of Eqs. (2.15) and (2.16), and would be more than adequate to eliminate leptons from semileptonic b decay [17,18]. With the leptonic cuts imposed, the jet-vetoing efficiency for this signal is about 70%.

Jet tagging can also be applied to the W^+W^+ process [16,17]. By tagging a forward jet and imposing a cut on

the minimum invariant mass of the tagged jet and a lepton, $M(lj_{\text{tag}}) > 200$ GeV, it is possible to further reduce the backgrounds. This tag is especially effective to reduce the $t\bar{t}$ cascade decay background since $M(lj_{\text{tag}})$ is significantly larger for the signal than for the background. However, since we assume that charged-lepton isolation can be implemented at the level required to eliminate the cascade decay background, we will not impose such a cut in this paper. Should a problem arise in experimentally implementing lepton isolation, this type of cut can be used as an alternative.

In Table I we list the kinematic cuts used in our study at the SSC (and LHC in parentheses). In Tables II(a) and II(b) we present the cross sections obtained in the SM from the electroweak processes at $m_H = 1$ and 0.1 TeV, as well as those for the $q\bar{q}$ annihilation continuum pair production (QCD) reactions. The results in the "leptonic cuts only" column are those obtained by imposing only the leptonic cuts of Table I, including the back-to-back cuts in the W^+W^- and $W^{\pm}W^{\pm}$ channels. In the next two columns, the cross sections obtained after imposing jet tagging and/or vetoing, *in addition to the leptonic cuts*, are given. The efficiencies at the SSC and LHC for the signal are obtained by taking the difference between the $m_H = 1$ and 0.1 TeV results. The branching ratios for each leptonic channel and the efficiencies for the signal when performing jet tagging and/or vetoing (with leptonic cuts already imposed) are summarized in Table III.

For other models of $W_L W_L$ interactions, we will proceed as follows. We first compute the cross sections for $W_L W_L$ production in a given model by using the

effective W approximation (EWA) [4,5] and the equivalence theorem (ET) [1–3]. In using the EWA, we compute total cross sections, subject leptonic cuts, ignoring all jet observables. To assess the inaccuracies that

TABLE I. Leptonic, tagging, and vetoing cuts on jets, by mode at the SSC (LHC).

ZZ leptonic cuts	Tag only
$\|y(l)\| < 2.5$	$E(j_{\text{tag}}) > 1.0$ (0.8) TeV
$p_T(l) > 40$ GeV	$3.0 < \|y(j_{\text{tag}})\| < 5.0$
$p_T(Z) > \frac{1}{4}\sqrt{M^2(ZZ) - 4M_Z^2}$	$p_T(j_{\text{tag}}) > 40$ GeV
$M(ZZ) > 500$ GeV	

W^+W^- leptonic cuts	Tag and veto
$\|y(l)\| < 2.0$	$E(j_{\text{tag}}) > 1.5$ (1.0) TeV
$p_T(l) > 100$ GeV	$3.0 < \|y(j_{\text{tag}})\| < 5.0$
$\Delta p_T(ll) > 450$ GeV	$p_T(j_{\text{tag}}) > 40$ GeV
$\cos\phi_{ll} < -0.8$	$p_T(j_{\text{veto}}) > 30$ GeV
$M(ll) > 250$ GeV	$\|y(j_{\text{veto}})\| < 3.0$

W^+Z leptonic cuts	Tag and veto
$\|y(l)\| < 2.5$	$E(j_{\text{tag}}) > 2.0$ (1.5) Tev
$p_T(l) > 40$ GeV	$3.0 < \|y(j_{\text{tag}})\| < 5.0$
$\not{p}_T > 75$ GeV	$p_T(j_{\text{tag}}) > 40$ GeV
$p_T(Z) > \frac{1}{4}M_T$	$p_T(j_{\text{veto}}) > 60$ GeV
$M_T > 500$ GeV	$\|y(j_{\text{veto}})\| < 3.0$

W^+W^+ leptonic cuts	Veto only
$\|y(l)\| < 2.0$	$p_T(j_{\text{veto}}) > 60$ GeV
$p_T(l) > 100$ GeV	$\|y(j_{\text{veto}})\| < 3.0$
$\Delta p_T(ll) > 200$ GeV	
$\cos\phi_{ll} < -0.8$	
$M(ll) > 250$ GeV	

TABLE II. Standard model cross sections (in fb) for $m_H = 1$ TeV, $m_H = 0.1$ TeV, and for the QCD background, with (a) $\sqrt{s} = 40$ TeV, $m_t = 140$ GeV, (b) $\sqrt{s} = 16$ TeV and $m_t = 140$ GeV.

(a) ZZ	Leptonic cuts only	Tag only	Veto plus tag
EW ($m_H = 1$ TeV)	1.2	0.68	
EW ($m_H = 0.1$ TeV)	0.17	0.07	
QCD	0.92	0.02	
W^+W^-		veto only	
EW ($m_H = 1$ TeV)	11	5.5	3.6
EW ($m_H = 0.1$ TeV)	2.2	0.49	0.30
QCD	15	15	0.31
$t\bar{t}j$	1300	14	1.5
W^+Z		veto only	
EW ($m_H = 1$ TeV)	1.3	0.41	0.21
EW ($m_H = 0.1$ TeV)	1.1	0.26	0.13
QCD	3.1	3.1	0.11
$Zt\bar{t}j$	1.4	0.04	0.01
W^+W^+		veto only	
EW ($m_H = 1$ TeV)	2.4	0.98	
EW ($m_H = 0.1$ TeV)	1.4	0.29	
QCD	0.24	0.01	
$Wt\bar{t}$	0.75	0.05	
(b) ZZ	leptonic cuts only	tag only	veto plus tag
EW ($m_H = 1$ TeV)	0.17	0.076	
EW ($m_H = 0.1$ TeV)	0.029	0.007	
QCD	0.33	0.003	
W^+W^-		veto only	
EW ($m_H = 1$ TeV)	1.6	0.52	0.31
EW ($m_H = 0.1$ TeV)	0.42	0.049	0.022
QCD	4.3	4.3	0.042
$t\bar{t}j$	107	1.5	0.12
W^+Z		veto only	
EW ($m_H = 1$ TeV)	0.25	0.059	0.022
EW ($m_H = 0.1$ TeV)	0.20	0.035	0.012
QCD	1.2	1.2	0.011
$Zt\bar{t}j$	0.085	0.003	0.000
W^+W^+		veto only	
EW ($m_H = 1$ TeV)	0.43	0.13	
EW ($m_H = 0.1$ TeV)	0.27	0.037	
QCD	0.063	0.003	
$Wt\bar{t}$	0.24	0.02	

TABLE III. WW leptonic branching ratios and the efficiencies of jet tagging and vetoing for the $W_L W_L$ signal at the SSC (LHC).

ZZ	Branching ratio	Tag only	Veto plus tag
	0.45%	59%(49%)	
$W^+ W^-$	Branching ratio	Veto only	Veto plus tag
	4.7%	57%(40%)	38%(24%)
$W^+ Z$	Branching ratio	Veto only	Veto plus tag
	1.5%	75%(48%)	40%(20%)
$W^+ W^+$	Branching raito	Veto only	Veto plus tag
	4.7%	69%(58%)	

might arise as a result of these approximations, we will make a detailed comparison between the EWA and ET computations and the exact SM calculation in Sec. IV. To implement the lepton cuts, including back-to-back requirements in the $W^+ W^-$ and $W^\pm W^\pm$ channels, we decay the final W_L's according to the appropriate angular distributions. The results will differ from the exact calculation to the extent that lepton cut efficiencies depend upon the p_T of the WW system. For the cuts employed, a comparison between the exact and EWA lepton cut efficiencies is made in Sec. IV for the 1-TeV SM Higgs case, and good agreement is found. To obtain cross sections in the EWA approximation that include the jet-tagging and jet-vetoing cuts, we will simply multiply the cross sections calculated from EWA by the net jet-tagging and/or jet-vetoing efficiency for each channel as computed for the $W_L W_L$ signal in the exact SM calculation with a 1-TeV Higgs boson. We believe that this procedure should be fairly accurate. Indeed, the kinematics of the jets in the signal events are determined by the kinematics of the initial W_L's that participate in the $W_L W_L$ scattering process. These kinematics are independent of the strong $W_L W_L$ scattering amplitude.

III. BEYOND THE STANDARD MODEL

In this section we present a variety of models that unitarize the $W_L W_L$ scattering amplitude. We start by reviewing the standard model and then discuss other possibilities that are consistent with all the data to date [33].

Let us begin by recalling that in the standard model, the $W_L W_L$ scattering amplitudes are unitarized by exchange of a spin-zero resonance, the Higgs particle H. The Higgs boson is contained in a complex scalar doublet:

$$\Phi = (v + H)\exp(2iw^a \tau^a / v) , \qquad (3.1)$$

where the τ^a are the generators of SU(2), normalized so that $\mathrm{Tr}\tau^a \tau^b = \delta^{ab}/2$. The four components of Φ contain three would-be Goldstone bosons w^a and the Higgs particle H. In the standard model, the Higgs potential

$$\mathcal{V} = \frac{\lambda}{16}[\mathrm{Tr}(\Phi^\dagger \Phi - v^2)]^2 \qquad (3.2)$$

is invariant under a rigid $\mathrm{SU}(2)_L \times \mathrm{SU}(2)_R$ symmetry:

$$\Phi \to L\Phi R^\dagger , \qquad (3.3)$$

with $L, R \in \mathrm{SU}(2)$. The vacuum expectation value

$$\langle \Phi \rangle = v \qquad (3.4)$$

breaks the symmetry to the diagonal SU(2). In the perturbative limit, it also gives mass to the Higgs boson:

$$m_H = \sqrt{2\lambda} v , \qquad (3.5)$$

where $v = 246$ GeV.

In the standard model, the diagonal SU(2) symmetry is broken only by terms proportional to the hypercharge coupling g' and the up-down fermion mass splittings. It is responsible for the successful mass relation

$$M_W = M_Z \cos\theta , \qquad (3.6)$$

where θ is the weak mixing angle; M_W and M_Z are the masses of $W^\pm$ and Z, respectively. The four components of Φ split into a triplet w^a and a singlet H under the SU(2) symmetry. In analogy to the chiral symmetry of QCD, we call the unbroken SU(2) "isospin."

At high energies, the scattering of longitudinally polarized W particles can be approximated by the scattering of the would-be Goldstone bosons w^a [1–3].

For the standard model, this is a calculational simplification, but for other models it is a powerful conceptual aid as well. For example, if one thinks of the would-be Goldstone fields in analogy with the pions of QCD, one expects the $W_L W_L$ scattering amplitudes to be unitarized by a spin-one, isospin-one vector resonance, such as the techni-ρ. Alternatively, if one thinks of the Goldstone fields in terms of the linear σ model, one expects the scattering amplitudes to be unitarized by a spin-zero, isospin-zero scalar field such as the Higgs boson.

In this paper, we are interested in the strongly interacting longitudinal W's in the TeV region. We will ignore the gauge couplings and the up-down fermion mass splittings. Therefore the SU(2) "isospin" is conserved. The $W_L W_L$ scattering amplitudes can then be written in terms of isospin amplitudes, exactly as in QCD. If we assign isospin indices

$$W_L^a W_L^b \to W_L^c W_L^d , \qquad (3.7)$$

then the scattering amplitude is given by

$$\begin{aligned}
\mathcal{M}(W_L^a W_L^b \to W_L^c W_L^d) =\ & A(s,t,u)\delta^{ab}\delta^{cd} \\
& + A(t,s,u)\delta^{ac}\delta^{bd} \\
& + A(u,t,s)\delta^{ad}\delta^{bc} ,
\end{aligned} \qquad (3.8)$$

where $a,b,c,d = 1,2,3$. [We use W_L to denote either $W_L^\pm$ or Z_L, where $W_L^\pm = (1/\sqrt{2})(W_L^1 \mp iW_L^2)$ and $Z_L = W_L^3$.] All the physics of $W_L W_L$ scattering is contained in the amplitude functions A.

Given the amplitude functions, the physical amplitudes for boson-boson scattering are given as

$$\mathcal{M}(W_L^+ W_L^- \to Z_L Z_L) = A(s,t,u) ,$$
$$\mathcal{M}(Z_L Z_L \to W_L^+ W_L^-) = A(s,t,u) ,$$
$$\mathcal{M}(W_L^+ W_L^- \to W_L^+ W_L^-) = A(s,t,u) + A(t,s,u) ,$$

$$(3.9)$$

$$\mathcal{M}(Z_L Z_L \to Z_L Z_L) = A(s,t,u) + A(t,s,u) + A(u,t,s) ,$$
$$\mathcal{M}(W_L^\pm Z_L \to W_L^\pm Z_L) = A(t,s,u) ,$$
$$\mathcal{M}(W_L^\pm W_L^\pm \to W_L^\pm W_L^\pm) = A(t,s,u) + A(u,t,s) .$$

In these expressions, the amplitudes do not include the symmetry factors for identical particles.

The isospin amplitudes $T(I)$, for isospin I, are given by

$$T(0) = 3A(s,t,u) + A(t,s,u) + A(u,t,s) ,$$

$$T(1) = A(t,s,u) - A(u,t,s) , \qquad (3.10)$$

$$T(2) = A(t,s,u) + A(u,t,s) .$$

In terms of the isospin amplitudes, the physical scattering amplitudes can be written

$$\mathcal{M}(W_L^+ W_L^- \rightarrow Z_L Z_L) = \tfrac{1}{3}[T(0) - T(2)] ,$$

$$\mathcal{M}(Z_L Z_L \rightarrow W_L^+ W_L^-) = \tfrac{1}{3}[T(0) - T(2)] ,$$

$$\mathcal{M}(W_L^+ W_L^- \rightarrow W_L^+ W_L^-) = \tfrac{1}{6}[2T(0) + 3T(1) + T(2)] ,$$

$$\mathcal{M}(Z_L Z_L \rightarrow Z_L Z_L) = \tfrac{1}{3}[T(0) + 2T(2)] , \qquad (3.11)$$

$$\mathcal{M}(W_L^\pm Z_L \rightarrow W_L^\pm Z_L) = \tfrac{1}{2}[T(1) + T(2)] ,$$

$$\mathcal{M}(W_L^\pm W_L^\pm \rightarrow W_L^\pm W_L^\pm) = T(2) .$$

Again, these amplitudes do not include the symmetry factors for identical particles.

For the standard model, the amplitude functions are easy to work out. They can be expressed by

$$A(s,t,u) = \frac{-m_H^2}{v^2} \left[1 + \frac{m_H^2}{s - m_H^2 + im_H\Gamma_H\theta(s)} \right] , \qquad (3.12)$$

where m_H and $\Gamma_H = 3m_H^3/32\pi v^2$ are the mass and width of the Higgs boson; $\theta(s)$ is the step function which takes the value one for $s > 0$ and zero otherwise. Note that we have included a Breit-Wigner width for the Higgs particle in the s channel. This is a violation of the equivalence theorem, which causes an increase in the rate in the resonant channels [34–36]. More discussion of this violation will appear later. We have not included the width in the nonresonant channels.

The standard model has the advantage that it is a renormalizable theory and that all amplitudes are perturbatively unitary as long as m_H is not too large. Of course, at $m_H = 1$ TeV, some small amount of unitarity violation occurs near the resonance. Nonetheless, the signal rates we obtain for $m_H = 1$ TeV provide a first characterization of what one might expect in the case where $W_L W_L$ interactions become strong.

There are many other models that provide alternative descriptions of electroweak symmetry breaking. (We shall only consider models without any open inelastic channels in $W_L W_L$ scattering.) Many of these models are effective theories, based on nonrenormalizable chiral Lagrangians for the WW sector. These models must be understood in the context of an energy expansion. Generally, such an expansion does not provide a unitary description for all energies. This is simply because the effective Lagrangian does not make explicit the new physics that must appear at some scale Λ, well above the WW mass region where it is to be employed. For the purposes of this paper, we must ensure that the effective theories are unitary for the WW masses of interest.

To check unitarity, we first write the scattering ampli-

tudes in terms of the isospin amplitudes $T(I)$. We then expand in partial waves according to the usual formula

$$T(I) = 32\pi \sum_{l=0}^{\infty} (2l+1)P_l(\cos\theta)a_l^I ,$$

$$a_l^I = \frac{1}{64\pi} \int_{-1}^{1} d(\cos\theta)P_l(\cos\theta)T(I) . \qquad (3.13)$$

Two-body elastic unitarity is equivalent to the statement $|a_l^I - i/2| = \tfrac{1}{2}$. In this paper we will require $\mathrm{Re}\,a_l^I < 1/2$ as our unitarity condition.

Among possible alternative models, there are several distinctions we can make. The first is whether or not a particular model is resonant in the $W_L W_L$ channel. If it is resonant, the model can be classified by the spin and isospin of the resonance. If it is not, the analysis is more subtle. Nonetheless, we shall see that all possibilities can be described in terms of two parameters. In this work, we will restrict our attention to models with spin-zero, isospin-zero resonances (such as Higgs boson) and spin-one, isospin-one resonances (such as the techni-ρ resonance), and nonresonant models.

A. Spin-zero, isospin-zero resonances

1. O(2N) model

The first model we discuss represents an attempt to describe the standard model Higgs boson in the nonperturbative domain. In the perturbatively coupled standard model, the mass of the Higgs boson is proportional to the square root of the scalar self-coupling λ. Heavy Higgs particles correspond to large values of λ. For $m_H \gtrsim 1$ TeV, naive perturbation theory breaks down, and one must take a more sophisticated approach.

One possibility for exploring the nonperturbative regime is to exploit the isomorphism between $\mathrm{SU}(2)_L \times \mathrm{SU}(2)_R$ and $\mathrm{O}(4)$ [37]. Using a large-N approximation, one can solve the $\mathrm{O}(2N)$ model for all values of λ, to leading order in $1/N$. The resulting scattering amplitudes can be parametrized by the scale Λ of the Landau pole. Large values of Λ correspond to small couplings λ and relatively light Higgs particles. In contrast, small values of Λ correspond to large λ and describe the nonperturbative regime.

The amplitude functions can be found via standard large-N techniques. In the limit $N \rightarrow \infty$, they are [38]

$$A(s,t,u) = \frac{16\pi^2 s}{16\pi^2 v^2 - sN[2 + \ln(\Lambda^2/|s|)] + i\pi\theta(s)} , \qquad (3.14)$$

where Λ is the physical cutoff and $\theta(s)$ is the step function defined below Eq. (3.12). The scale of the cutoff completely determines the theory.

It is not hard to show that the $W_L W_L$ scattering amplitudes respect the unitarity condition for all energies $E \lesssim \Lambda$. In this paper we will take $N = 2$ and $\Lambda = 3$ TeV to characterize the strongly coupled standard model. If we parametrize the position of the pole by its "mass" m and "width" Γ through the relation $s = [m - (i/2)\Gamma]^2$, then $m \sim 0.8$ TeV and $\Gamma \sim 600$ GeV.

2. Chirally coupled scalar model

The second model describes the low-energy regime of a technicolor-like model whose lowest resonance is a techni-σ. The effective Lagrangian for such a resonance can be constructed using the techniques of Ref. [39]. The resulting Lagrangian is consistent with the chiral symmetry SU(2)$_L$ × SU(2)$_R$, spontaneously broken to the diagonal SU(2).

In this approach, the basic fields are $\Sigma = \exp(2iw^a\tau^a/v)$ and a scalar S. These fields transform as follows under SU(2)$_L$ × SU(2)$_R$:

$$\Sigma \to L\Sigma R^\dagger, \quad S \to S \ . \tag{3.15}$$

This is all we need to construct the effective Lagrangian. To the order of interest, it is given by

$$\mathcal{L}_{\text{scalar}} = \frac{v^2}{4}\,\text{Tr}\,\partial^\mu\Sigma^\dagger\partial_\mu\Sigma + \tfrac{1}{2}\partial^\mu S\,\partial_\mu S$$
$$- \tfrac{1}{2}M_S^2 S^2 + \tfrac{1}{2}gvS\,\text{Tr}\,\partial^\mu\Sigma^\dagger\partial_\mu\Sigma + \cdots \ , \tag{3.16}$$

where M_S is the isoscalar mass and g is related to its partial width into the Goldstone fields:

$$\Gamma_S = \frac{3g^2M_S^3}{32\pi v^2} \ . \tag{3.17}$$

To this order, the Lagrangian (3.16) is the most general chirally symmetric coupling of a spin-zero isoscalar resonance to the fields w^a. It contains two free parameters, which can be traded for the mass and the width of the S. For $g = 1$, the S reduces to an ordinary Higgs boson. For $g \neq 1$, however, the S is *not* a typical Higgs boson. It is simply an isoscalar resonance of arbitrary mass and width. In either case, one must be sure to check that the scattering amplitudes are unitary up to the energy of interest.

The tree-level scattering amplitude is easy to construct. It has two terms. The first is a direct four-Goldstone-boson coupling which ensures that the scattering amplitude satisfies the low-energy theorems (LET's) [40]. The second contains the contributions from the isoscalar resonance. Taken together, they give the full scattering amplitude:

$$A(s,t,u) = \frac{s}{v^2} - \left[\frac{g^2s^2}{v^2}\right]\frac{1}{s - M_S^2 + iM_S\Gamma_S\theta(s)} \ . \tag{3.18}$$

In what follows, we will choose $M_S = 1.0$ TeV, $\Gamma_S = 350$ GeV. These values give unitary scattering amplitudes up to 2 TeV. (We use the Breit-Wigner prescription to handle the s-channel resonance. Our criterion is to have all the partial waves respect the unitary condition up to 2 TeV except near the resonance; the slight unitarity violation near the resonance is due to the perturbative expansion of the width [34–36].)

B. Spin-one, isospin-one resonances

1. Chirally coupled vector model

This example provides a relatively model-independent description of the techni-ρ resonance that arises in most

technicolor theories. As above, one can use the techniques of nonlinear realizations to construct the most general coupling consistent with chiral symmetry [39,41–43].

To find the techni-ρ Lagrangian, we first parametrize the Goldstone fields w^a in a slightly different way:

$$\xi = \exp(iw^a\tau^a/v) \ , \tag{3.19}$$

and so $\Sigma = \xi^2$. We then represent an SU(2)$_L$ × SU(2)$_R$ transformation on the field ξ as

$$\xi \to \xi' \equiv L\xi U^\dagger = U\xi R^\dagger \ . \tag{3.20}$$

Here L, R, and U are SU(2) group elements and U is a (nonlinear) function of L, R, and w^a, chosen to restore ξ' to the form (3.19). Note that when $L = R$, $U = L = R$, and the transformation linearizes. This simply says that the w^a transform as a triplet under the diagonal SU(2).

Given these transformations, one can construct the currents

$$J_{\mu L} = \xi^\dagger\partial_\mu\xi \to UJ_{\mu L}U^\dagger + U\partial_\mu U^\dagger \ ,$$
$$J_{\mu R} = \xi\partial_\mu\xi^\dagger \to UJ_{\mu R}U^\dagger + U\partial_\mu U^\dagger \ . \tag{3.21}$$

The currents $J_{\mu L}$ and $J_{\mu R}$ transform as gauge fields under transformations in the diagonal SU(2). As above, the transformations linearize when $L = R = U$.

The transformations (3.21) inspire us to choose the techni-ρ transformation as

$$V_\mu \to UV_\mu U^\dagger + ig^{-1}U\,\partial_\mu U^\dagger \ . \tag{3.22}$$

In this expression, $V_\mu = V_\mu^a\tau^a$ and g is the techni-ρ coupling constant. When $L = R = U$, Eq. (3.22) implies that the techni-ρ transforms as an isotriplet of weak isospin.

Using these transformations, it is easy to construct the most general Lagrangian consistent with chiral symmetry. We first write down the currents

$$\mathcal{A}_\mu = J_{\mu L} - J_{\mu R} \ ,$$
$$\mathcal{V}_\mu = J_{\mu L} + J_{\mu R} + 2igV_\mu \ , \tag{3.23}$$

which transform as follows under an arbitrary chiral transformation:

$$\mathcal{A}_\mu \to U\mathcal{A}_\mu U^\dagger, \quad \mathcal{V}_\mu \to U\mathcal{V}_\mu U^\dagger \ . \tag{3.24}$$

Under parity (which exchanges J_L with J_R and leaves V invariant), $\mathcal{V}$ is invariant, while $\mathcal{A}$ changes sign. If we make the additional assumption that the underlying dynamics conserve parity, we are led to the Lagrangian

$$\mathcal{L}_{\text{vector}} = -\tfrac{1}{4}V_{\mu\nu}^a V^{a\mu\nu} - \tfrac{1}{4}v^2\,\text{Tr}\mathcal{A}_\mu\mathcal{A}^\mu$$
$$- \tfrac{1}{4}av^2\,\text{Tr}\mathcal{V}_\mu\mathcal{V}^\mu + \cdots \ , \tag{3.25}$$

where $V_{\mu\nu}^a$ is the (non-Abelian) field strength for the vector field V_μ^a. The dots in this equation denote terms with more derivatives. Up to a possible field redefinition, this is the most general coupling of a techni-ρ resonance to the Goldstone bosons, consistent with SU(2)$_L$ × SU(2)$_R$ symmetry.

In this Lagrangian, the parameter v is fixed as before.

The parameters g and a, however, are free. One combination is determined by the mass of the techni-ρ,

$$M_V^2 = ag^2v^2 \ , \tag{3.26}$$

and another by its width into techni-pions (i.e., Goldstone bosons),

$$\Gamma_V = \frac{aM_V^3}{192\pi v^2} \ . \tag{3.27}$$

Because of the chiral symmetry, these two parameters completely define the theory. As above, the scattering amplitude is easy to compute.

It contains a direct four-Goldstone-boson coupling, as well as the isovector resonance. One finds

$$A(s,t,u) = \frac{s}{4v^2}\left[4-3a\right]$$
$$+ \frac{aM_V^2}{4v^2}\left[\frac{u-s}{t-M_V^2+iM_V\Gamma_V\theta(t)}\right.$$
$$\left. + \frac{t-s}{u-M_V^2+iM_V\Gamma_V\theta(u)}\right] \ . \tag{3.28}$$

In what follows we will choose $M_V = 2.0$ TeV, $\Gamma_V = 700$ GeV and $M_V = 2.5$ TeV, $\Gamma_V = 1300$ GeV. These values preserve unitarity up to 3 TeV, except for a small unitarity violation near the s-channel resonance in the a_1^1 partial wave. Additional constraints can be found from precision measurements of the electroweak parameters. Our choices are consistent with current limits [43].

C. Nonresonant models

Effective field theories provide a useful formalism for describing resonances in $W_L W_L$ scattering beyond the

standard model. They also can be used to describe nonresonant models in which the $W_L W_L$ scattering occurs below the threshold for resonance production. The effective Lagrangian description allows one to construct scattering amplitudes that are consistent with crossing, unitarity, and chiral symmetry [44].

The most important effects at SSC energies can be found by considering the Lagrangian for the Goldstone fields:

$$\mathcal{L}_{\text{Goldstone}} = \frac{v^2}{4} \text{Tr}\partial_\mu \Sigma^\dagger \partial^\mu \Sigma$$
$$+ L_1\left[\frac{v}{\Lambda}\right]^2 \text{Tr}(\partial_\mu \Sigma^\dagger \partial^\mu \Sigma)\,\text{Tr}(\partial_\nu \Sigma^\dagger \partial^\nu \Sigma)$$
$$+ L_2\left[\frac{v}{\Lambda}\right]^2 \text{Tr}(\partial_\mu \Sigma^\dagger \partial_\nu \Sigma)\,\text{Tr}(\partial^\mu \Sigma^\dagger \partial^\nu \Sigma) \ , \tag{3.29}$$

where $\Lambda \lesssim 4\pi v$ denotes the scale of the new physics. To this order, this is the most general $\text{SU}(2)_L \times \text{SU}(2)_R$ invariant Lagrangian for the Goldstone fields [45,46].

The Lagrangian (3.29) describes new physics at energies below the mass of lightest new particles. All the effects of the new physics are contained in the coefficients of the higher-dimensional operators built from the Goldstone fields. To order p^2 in the energy expansion, only one operator contributes, and its coefficient is universal. To order p^4, however, there are two additional operators that contribute to $W_L W_L$ scattering.

To order p^4, the scattering amplitudes are given by

$$A(s,t,u) = \frac{s}{v^2} + \frac{1}{4\pi^2 v^4}[2L_1(\mu)s^2 + L_2(\mu)(t^2+u^2)]$$
$$+ \frac{1}{16\pi^2 v^4}\left[-\frac{t}{6}(s+2t)\ln\left[-\frac{t}{\mu^2}\right] - \frac{u}{6}(s+2u)\ln\left[-\frac{u}{\mu^2}\right] - \frac{s^2}{2}\ln\left[-\frac{s}{\mu^2}\right]\right] \ , \tag{3.30}$$

where we have taken $\Lambda = 4\pi v \sim 3.1$ TeV and the $L_i(\mu)$ are the renormalized coefficients in the effective Lagrangian $[\ln(-s) = \ln(s) - i\pi$, for $s > 0]$. To this order, there are two types of contributions. The first is a direct coupling that follows from the tree-level Lagrangian. The second is a one-loop correction that must be included at order p^4. The loop contribution renormalizes the parameters L_1 and L_2, and gives finite logarithmic corrections that cannot be absorbed into a redefinition of the couplings.

The difficulty with this approach is that at SSC energies the scattering amplitudes violate unitarity between 1 and 2 TeV. This indicates that new physics is near, but there is no guarantee that new resonances lie within the reach of the SSC. We choose to treat the uncertainties of

unitarization in three ways.

(1) We take $L_1(\mu) = L_2(\mu) = 0$ and ignore the loop-induced logarithmic corrections to the scattering amplitudes. The resulting amplitudes are universal in the sense that they depend only on v. They reproduce the low-energy theorems of pion dynamics. We unitarize these amplitudes by saturating the partial waves when they reach the bound $|a_I^J| \leq 1$.

This is the original model considered by Chanowitz and Gaillard (CG) [2], and so we call it the CG LET.

(2) For comparison, we consider another model in which we take $L_1(\mu) = L_2(\mu) = 0$ and ignore the loop-induced logarithmic corrections. This time, however, we unitarize the scattering amplitudes using a "K matrix"; that is, we replace the partial-wave amplitudes a_I^J by t_I^J,

where

$$t_l^I = \frac{a_l^I}{1 - i a_l^I} \ .$$ (3.31)

We call this model the K LET.

(3) The third nonresonant model we consider includes the full $O(p^4)$ amplitude presented above. By varying the parameters $L_1(\mu)$ and $L_2(\mu)$, one can sweep over all possible nonresonant physics. In particular, one can search for a region where unitarity violation is delayed up to 2 TeV. Scanning the $(L_1(\mu), L_2(\mu))$ parameter space, one finds that the values

$$L_1(\mu) = -0.26, \quad L_2(\mu) = +0.23 \ ,$$ (3.32)

measured at the renormalization scale $\mu = 1.5$ TeV, delay unitarity breakdown until 2 TeV. With these parameters, the amplitudes (3.30) are unitary, chiral, and crossing symmetric for energies up to 2 TeV. Beyond 2 TeV, the partial waves are no longer unitary. In order to compare with the total event rates in the other models, we unitarize the scattering amplitudes using the K-matrix prescription and so we call this model the K delay. Note that only the real part of a_l^I, from (3.13) and (3.30), is used to obtain the unitarized partial-wave amplitude t_l^I.

In what follows we use these models to represent new physics that is not resonant at SSC and LHC energies.

IV. NUMERICAL RESULTS

We now turn to the background and signal results for the models discussed in Secs. II and III. We begin by briefly summarizing our procedures and assumptions and then estimate the overall systematic error associated with the event rates to be presented.

In all our results, we use the leading-order parton distributions of Morfin and Tung [47], and include only the first four quark flavors as partons. In particular, we ignore the bottom quark as an initial-state parton. In computing signal event rates, we evaluate the parton distribution functions at the scale M_W. As discussed in Ref. [48], the agreement between the exact $W_L W_L$ production rates and those predicted by the effective-W approximation is best for this (natural) choice of scale. In a recent analysis that includes the next-order QCD corrections [49], it was found that for this choice of scale the QCD corrections to the WW scattering processes are very small, which indicates that the current tree-level calculations for the signals are rather reliable. The scales used in the background calculations depend upon the process and are given in the references quoted in Sec. II. In general, the choices of scale are either strongly motivated on theoretical grounds or are those leading to the smallest higher-order corrections. To estimate the systematic error that is associated with our background rates because of scale choice and higher-order corrections, we need higher-order calculations which are not available at present. In the TeV region, however, the typical scales are large. This makes the strong coupling small and takes the parton distribution functions into regimes of relatively large momentum fraction, which are well represented by experimental data.

To check the accuracy of employing the effective-W approximation in combination with the equivalence

theorem (EWA/ET), we present a comparison in Table IV. For the test case of the standard model with a 1-TeV Higgs boson, the agreement between this approximation technique (EWA/ET) and the "subtraction" result using the full SM matrix-element calculation (subtraction) is reasonably good and generally becomes best at large invariant mass of the final state WW pair. However, in the W^+W^+ final state the agreement is excellent for all mass cuts examined. For other channels, the discrepancy at lower $M(WW)$ potentially derives from two sources: (a) use of the EWA for the longitudinally polarized W-boson scattering amplitudes and (b) unavoidable inconsistencies associated with implementing the equivalence theorem, leading to a difference between EWA/ET and EWA/LL. (The EWA/LL approximation is that in which the EWA is employed in conjunction with the full longitudinal W-boson scattering amplitudes.) Regarding (a), we note that the derivation of the EWA intrinsically relies on $M(WW)$ being large. Thus it is natural that some deviation between the subtraction and EWA computations for the $W_L W_L$ final state could appear at low WW invariant mass. However, the close agreement between the exact and EWA/ET results for the W^+W^+ channel suggest that this source of deviation is quite small. This is because W^+W^+, being nonresonant, does not suffer from difficulties of type (b). Indeed, good agreement between exact and EWA/LL calculations for the (opposite charge) W^+W^- channel has been found in earlier work [50] where the ET approximation was not employed. The main difference of type (b), i.e., between EWA/LL and EWA/ET, arises from our procedure of employing the Breit-Wigner prescription for s-channel resonances. As discussed below, if this procedure is employed (in the SM) for both a direct calculation of $W_L W_L \rightarrow W_L W_L$ using true W-boson fields and in the ET calculation of the same process, a large discrepancy is found for $M(WW)$ below

TABLE IV. SM signal cross section comparison between the subtraction results of Eq. (2.2) and the EWA/ET results ($m_H = 1$ TeV) at the SSC, $\sqrt{s} = 40$ TeV, in units of fb. Only the leptonic cuts in Table I are imposed.

	Subtraction	EWA/ET SM
ZZ		
$M_{ZZ} > 0.5$	1.0	1.9
$M_{ZZ} > 1.0$	0.52	0.69
$M_{ZZ} > 1.5$	0.06	0.08
W^+W^-		
$M_{ll} > 0.25$	9.0	12.6
$M_{ll} > 0.5$	7.8	12.1
$M_{ll} > 1.0$	0.68	1.0
W^+Z		
$M_T > 0.5$	0.29	0.33
$M_T > 1.0$	0.17	0.13
$M_T > 1.5$	0.08	0.05
W^+W^+		
$M_{ll} > 0.25$	0.90	0.93
$M_{ll} > 0.5$	0.47	0.46
$M_{ll} > 1.0$	0.10	0.10

the Higgs boson mass. The net deviation between the full matrix-element calculation, as defined in Eq. (2.2), and the EWA/ET is displayed in Table IV.

Let us discuss briefly the inconsistencies associated with employing the Breit-Wigner prescription for the s-channel resonances in the scattering amplitudes. These were studied in the case of a heavy SM Higgs boson in Ref. [35]. As already noted, the Breit-Wigner procedure for putting the width into the directly computed $W_L W_L \rightarrow W_L W_L$ amplitudes with true longitudinally polarized gauge bosons does not yield the same result as the identical procedure in the equivalence-theorem calculation. However, it is easily demonstrated that this violation of the equivalence theorem is higher order in the perturbation expansion. When the width is small, the perturbative expansion is valid and the violation is tiny. For large width, the Breit-Wigner procedure yields a significant violation of the equivalence theorem for

$M(WW)$ below the resonance mass, but an unambiguous treatment is impossible because the perturbative expansion is breaking down. Our procedure can simply be viewed as defining a particular model for $W_L W_L$ production. The second effect of adding the width through the Breit-Wigner prescription is to give a small violation of unitarity in the partial waves which contain the resonance. This can again be traced to a breakdown of the perturbative calculation and the Breit-Wigner induced violation of the equivalence theorem. This small violation of unitary near the resonance can be safely ignored. Much more important is our demand that the unitarity conditions hold away from the resonance, in particular up to the highest $M(WW)$ scale of interest. Indeed, our cuts automatically emphasize the large $M(WW)$ region in which the Breit-Wigner procedure becomes immaterial. Thus, as already stated, we see no reason to anticipate large errors in our signal rates in the large $M(WW)$ re-

TABLE V. (a) Event rates per SSC year, assuming $m_t = 140$ GeV, $\sqrt{s} = 40$ TeV, and an annual luminosity of 10 fb^{-1}. Cuts are listed in Table I. (b) Event rates per LHC year, assuming $m_t = 140$ GeV, $\sqrt{s} = 16$ TeV, and an annual luminosity of 100 fb^{-1}. Cuts are listed in Table I.

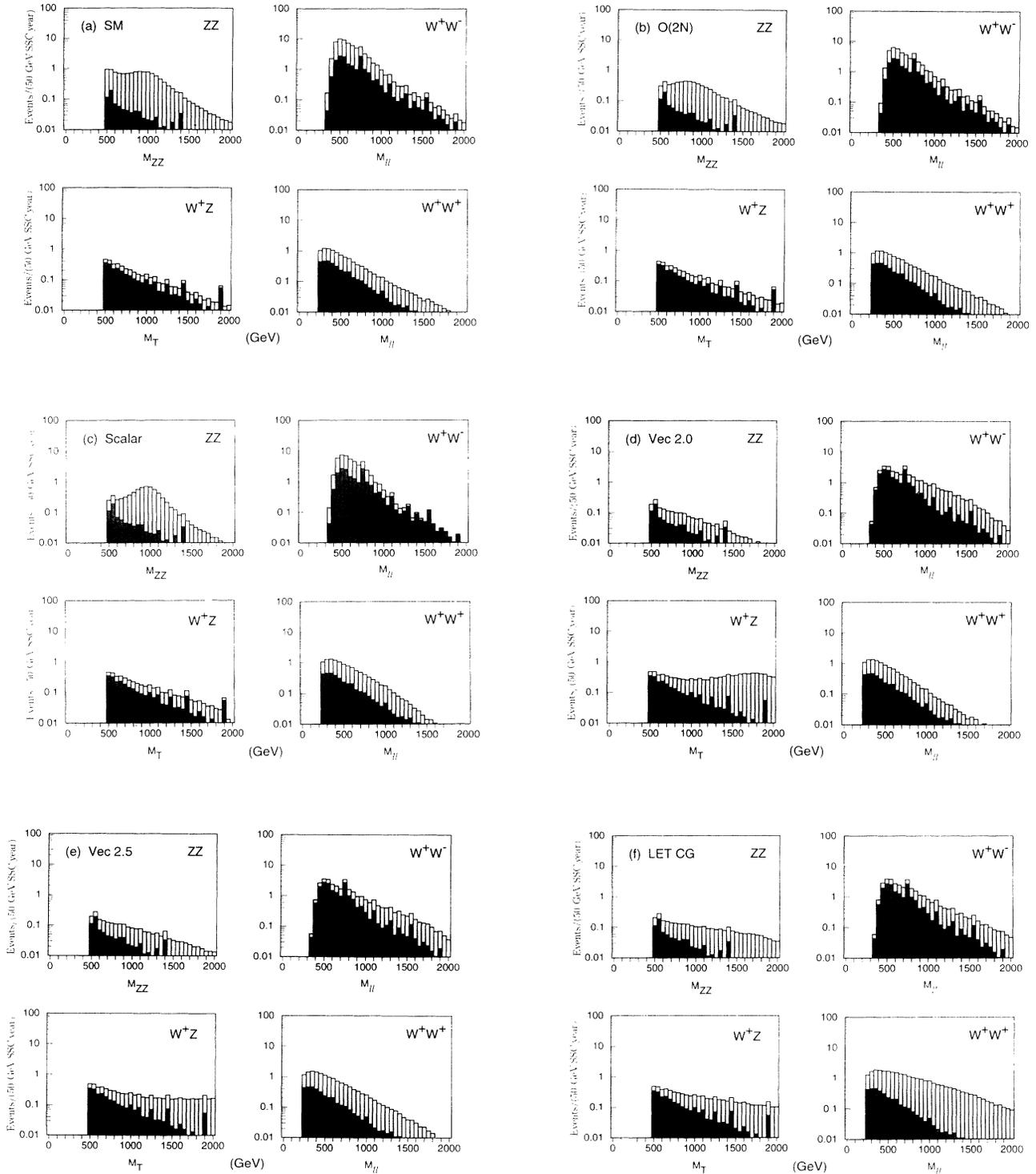|	Bkgd.	SM	Scalar	O(2N)	Vec. 2.0	Vec. 2.5	CG LET	K LET	K delay
					(a)				
ZZ									
$M_{ZZ} > 0.5$	1.0	11	6.2	5.2	1.1	1.5	2.6	2.2	1.6
$M_{ZZ} > 1.0$	0.3	4.1	2.6	2.0	0.4	0.7	1.6	1.3	0.8
$M_{ZZ} > 1.5$	0.1	0.5	0.2	0.5	0.1	0.3	0.9	0.6	0.4
W^+W^-									
$M_{ll} > 0.25$	21	48	30	24	15	12	16	12	11
$M_{ll} > 0.5$	17	46	29	23	15	12	15	11	11
$M_{ll} > 1.0$	3.6	3.8	1.1	2.7	6.5	4.9	5.3	3.6	4.6
W^+Z									
$M_T > 0.5$	2.5	1.3	1.8	1.5	9.5	6.2	5.8	4.9	6.0
$M_T > 1.0$	0.8	0.5	0.8	0.7	7.9	4.7	4.1	3.3	4.6
$M_T > 1.5$	0.3	0.2	0.2	0.3	5.5	3.2	2.6	1.9	3.2
W^+W^+									
$M_{ll} > 0.25$	3.5	6.4	8.2	7.1	7.8	11	25	21	15
$M_{ll} > 0.5$	1.5	3.2	4.2	3.9	3.8	6.3	19	15	11
$M_{ll} > 1.0$	0.2	0.7	0.6	0.9	0.5	1.2	7.6	5.2	5.2
					(b)				
ZZ									
$M_{ZZ} > 0.5$	1.0	14	7.5	6.4	1.4	1.7	2.5	2.2	1.8
$M_{ZZ} > 1.0$	0.1	3.9	2.7	1.8	0.4	0.6	1.1	0.9	0.6
$M_{ZZ} > 1.5$	0.0	0.3	0.1	0.3	0.1	0.2	0.4	0.3	0.2
W^+W^-									
$M_{ll} > 0.25$	18	40	26	19	8.0	6.8	9.2	7.2	6.2
$M_{ll} > 0.5$	15	32	21	16	7.4	6.1	8.3	6.3	5.5
$M_{ll} > 1.0$	2.5	1.3	0.4	1.0	2.4	1.6	1.7	1.1	1.2
W^+Z									
$M_T > 0.5$	2.4	1.0	1.4	1.1	4.8	3.2	3.2	2.9	3.0
$M_T > 1.0$	0.3	0.3	0.4	0.3	3.3	1.8	1.6	1.4	1.7
$M_T > 1.5$	0.1	0.1	0.1	0.1	2.0	1.0	0.8	0.6	0.9
W^+W^+									
$M_{ll} > 0.25$	6.2	9.6	12	10	12	16	27	24	16
$M_{ll} > 0.5$	1.7	3.7	5.2	4.3	4.8	7.3	16	14	8.3
$M_{ll} > 1.0$	0.2	0.4	0.5	0.6	0.4	1.0	4.2	2.9	2.3

J. BAGGER *et al.*

FIG. 3. Invariant mass distributions for the "gold-plated" leptonic final states that arise from the processes $pp \to ZZX$, $pp \to W^+W^-X$, $pp \to W^+ZX$, and $pp \to W^+W^+X$, for $\sqrt{s} = 40$ TeV and an annual SSC luminosity of 10 fb^{-1}. The longitudinally polarized signal is plotted above the summed background. The mass variable of the x axis is in units of GeV, and the bin size is 50 GeV. (a) SM with a 1-TeV Higgs boson; (b) O(4) model with $\Lambda = 3$ TeV; (c) chirally coupled scalar with $M_S = 1$ TeV, $\Gamma_S = 350$ GeV; (d) chirally coupled vector with $M_V = 2$ TeV, $\Gamma_V = 700$ GeV; (e) chirally coupled vector with $M_V = 2.5$ TeV, $\Gamma_V = 1300$ GeV; (f) nonresonant model unitarized following Chanowitz and Gaillard; (g) nonresonant model unitarized by the K-matrix prescription; (h) $O(p^4)$ nonresonant model with delayed unitarity violation, unitarized by the K-matrix prescription.
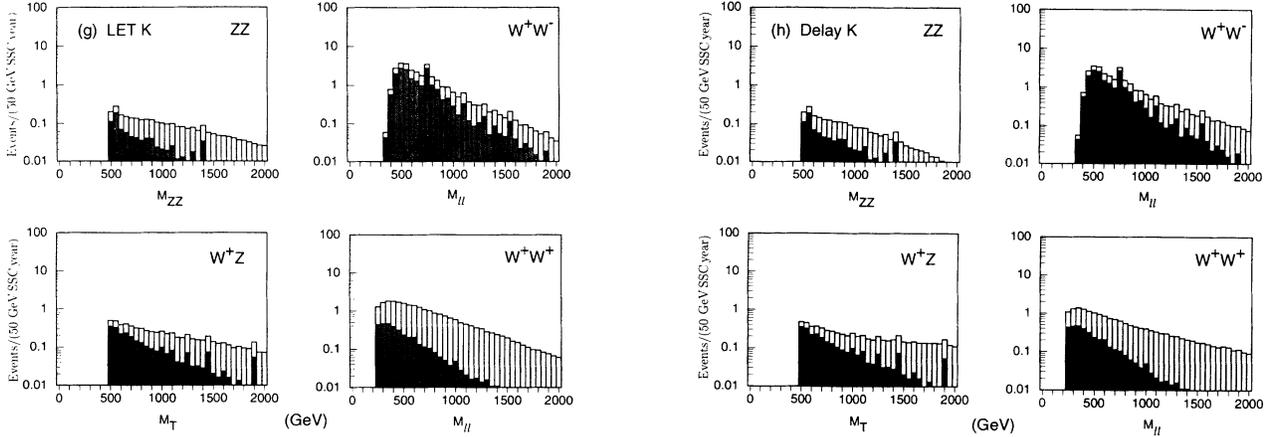
FIG. 3. (*Continued*).

gion.

Finally, we remind the reader that our *signal* is defined as the number of $W_L W_L$ pairs produced in any given channel. In general, this is not the same as one would obtain by plotting events as a function of $M(WW)$ and then subtracting a smooth background under some "bump" in the distribution. Even in the fully reconstructable four-lepton final state of the ZZ channel, a spin-zero isospin-zero resonance is significantly above the continuum background at high $M(ZZ)$, well beyond the obvious bump in the distribution. Indeed, in nonresonant channels, such as $W^+ W^+$, there is no visible bump in $M(WW)$. And, for most of the final states considered, the missing neutrinos make full reconstruction of the WW mass impossible in any case. The ability to detect the signal will thus ultimately depend upon the accuracy with which the expected rate for WW production in the LT and TT polarization modes can be computed. As we have already emphasized, the SM computation (with a light Higgs boson) gives an accurate result for this rate.

The signal and background rates that we shall quote are only as good as the parton distributions and parton-level Monte Carlo programs employed. Significant improvements in both will be made once data from the DESY *ep* collider HERA are available. Also, the required parton distributions will be determined to high accuracy by other high-p_T and Drell-Yan pair measurements at the SSC or LHC, and implementation of the cuts by each detector collaboration will become very well understood as experience with the apparatus accumulates and the full hadronic-level Monte Carlo simulations are fine-tuned at SSC and/or LHC energies. In particular, the background levels in the various channels should become sufficiently well determined that any significant LL (i.e., $W_L W_L$) excess will be evident. Although at present we are confined to parton-level predictions, our results should give a reliable indication of the ultimate rates for the background and signal that can be achieved in each model after appropriate cuts.

We summarize our results in Tables V(a) and V(b) for the SSC and LHC, respectively. These tables give the event rates for the summed background and for the signal

in each of the models as a function of the mass cut placed on the final state. The particular type of mass cut is channel dependent and has been detailed in Sec. II. For each channel, the second mass cut for which we tabulate results is the minimum for which we deem the EWA/ET approximation to be reliable for all the different models. For instance, in the case of the SM, scalar model, and O($2N$) model, the optimal cut on $M(ll)$ in the $W^+ W^-$ channel is of order 500 GeV. For such a cut, contributing $M(WW)$ values are large enough that the EWA/ET approximation is quite good. Results for other cuts illustrate how rapidly the event levels fall off with increasing invariant mass cut. Lower cuts might be reliable for some channels in the case of some models. For instance, in the $W^+ W^-$ channel, the CG LET, K LET, and K delay models all lack resonance structure of any kind, and the EWA/ET approximation might be adequate for $M(ll) \gtrsim 250$ GeV. In Fig. 3 we show distributions in the mass variables for several different models at the SSC. Of course, the number of events expected (see the tables) is generally much too small to allow for an actual measurement of these mass distributions. However, the distributions allow for some intuitive feeling as to where the signal event rates are largest and how rapidly the rates decline with increasing invariant mass.

From the tables it is apparent that the absolute number of (leptonic channel) signal events in one SSC year (10 fb^{-1}) or one LHC year (100 fb^{-1}) is never large. However, our cuts have reduced backgrounds to a remarkably low level, so that even a relatively small number of excess LL events should be observable. Consequently, we find that for each model, whether it has a scalar resonance, a vector resonance, or no resonance at all, there is always a WW charged-lepton mode for which the signal is larger than background. For instance, for the SM, the scalar resonance model, and the O($2N$) model, the electroweak symmetry-breaking sector contains a spin-zero isospin-zero resonance. As a result, the signal rates in the ZZ and $W^+ W^-$ channels are clearly above the background. Similarly, the signal event rate in the $W^+ Z$ mode is larger than the background rate for the two vector models with a spin-one isospin-one resonance. Finally, the

TABLE VI. Number of years (if < 10) at SSC required (a) for a 99% confidence level signal; (b) for a 95% confidence level signal.

Model Channel	SM	Scalar	O(2N)	Vec. 2.0	Vec. 2.5	CG LET	K LET	K delay
					(a)			
ZZ	2.2	4.0	5.8			7.8		
W^+W^-	0.50	1.0	1.2	2.5	3.5	2.5	4.0	4.0
W^+Z				1.5	2.8	3.2	4.2	2.8
W^+W^+	6.2	4.0	4.5	4.8	2.2	0.50	0.75	1.2
				(b)				
ZZ	1.2	2.2	3.0			4.0	5.5	
W^+W^-	0.25	0.50	0.75	1.2	1.8	1.2	2.0	2.0
W^+Z				0.75	1.5	1.8	2.2	1.5
W^+W^+	3.2	2.2	2.2	2.5	1.2	0.25	0.50	0.50

W^+W^+ mode has the most significant event rate in the CG LET, K LET, and K delay models that have no resonance.

To quantify the observability of a given signal above background, we proceed as follows. We define the signal to be observable at a confidence level of $P\%$ if the maximum number of background events, B_{max} at $P\%$ confidence level is smaller than the minimum number of signal plus background events, SB_{min}, at $P\%$ confidence level. Here B_{max} is the number of background events such that the probability of having any number up to and including B_{max} is $0.01P$, while SB_{min} is the number of signal plus background events such that the probability of having a number greater than or equal to SB_{min} is $0.01P$. For a 99% confidence level signal, these two probabilities are 0.99. The values B_{max} and SB_{min} are computed assuming Poisson statistics. For integer values, this means that we require[1]

$$0.01P = \sum_{n=0}^{B_{max}} \frac{B^n}{n!} e^{-B},$$

$$0.01P = \sum_{n=SB_{min}}^{\infty} \frac{(S+B)^n}{n!} e^{-(S+B)},$$

(4.1)

where B and $S+B$ are the background and signal plus background rates, respectively. B and S are obtained as a function of luminosity from the event rates tabulated earlier for the different types of models by scaling with respect to the luminosities of 10 and 100 fb^{-1} adopted for the SSC and LHC, respectively, in constructing the tables. We will uniformly employ results for the middle (second) mass cut tabulated for each channel. Even though backgrounds decrease rapidly with increasing invariant mass cut, the signal also decreases (though less rapidly) and the limited resulting statistics are such that

there is no channel for which the higher (third) mass cut tabulated in Tables V(a) and V(b) leads to a more observable signal at either the 99% or 95% confidence level.

As an example, consider again the W^+W^- channel and the SM, scalar model, and O(2N) model (for integrated luminosity of 10 fb^{-1} at the SSC). For all three models, the background rate of 17 events is smaller than the signal rates. The smallest signal rate among the three models for the $M_{ll} \geq 0.5$ TeV cut is the 23 events predicted for the O(2N) model. The 99% confidence level upper limit on the background is 27 events, whereas for the O(2N) model the 99% confidence level lower limit on signal plus background is 25 events. Thus the predicted signal is not quite observable at the 99% confidence level for the O(2N) model. In contrast, 99% confidence level is achieved for the SM and scalar model in the W^+W^- channel after (less than) one 10 fb^{-1} year.

The simplest manner in which the observability of all the various signals can be tabulated is to give the number of years required to achieve a signal at a given confidence level for each channel and each model. (Of course, if the machine can be run at a higher instantaneous luminosity the required integrated luminosities can be achieved in less than the time indicated.) These results for the SSC and LHC appear in Tables VI and VII, respectively. Let us first discuss the SSC results. In Table VI(a) [VI(b)] we give the number of 10 fb^{-1} year required to see a signal in a given channel for a given model at a 99% (95%) confidence level, as defined above. As indicated earlier, the clearest signals for the SM, scalar model, and O(2N) model are obtained in the W^+W^- channel. The vector models are most easily probed in the W^+Z channel. (Note, however, that for the vector 2.5 model, the W^+W^+ channel is actually superior after imposing the kinematic cuts listed in Table I.) Finally, the CG LET, K LET, and K delay models are only readily probed using the W^+W^+ channel. This is not to say that other channels are useless, especially if a 95% confidence level signal is deemed adequate. Relatively small numbers of years (<2.5) are required to observe a signal at 95% confidence level in all cases except: the W^+Z channel for the SM, scalar model, and O(2N) model, the ZZ channel for the O(2N), vector, and LET/delay models; and the

---

[1]If the equalities in Eq. (4.1) are not satisfied for integer values of B_{max} and SB_{min}, we determine B_{max} and/or SB_{min} by interpolating between the two integer values such that the appropriate sum is just below and just above $0.01P$.

TABLE VII. Number of years (if < 10) at LHC required (a) for a 99% confidence level signal; (b) for a 95% confidence level signal.

Channel/model	SM	Scalar	O(2N)	Vec. 2.0	Vec. 2.5	CG LET	K LET	K delay
				(a)				
ZZ	2.0	3.0	4.8			9.0		
W^+W^+	0.75	1.2	2.0	7.5		6.0		
W^+Z				3.0	6.8	7.8	9.5	7.2
W^+W^+	5.2	3.2	4.2	3.5	2.0	0.75	0.75	1.8
				(b)				
ZZ	1.2	1.8	2.5			4.8	6.0	
W^+W^-	0.50	0.75	1.0	3.8	5.2	3.0	5.0	6.5
W^+Z				1.8	3.5	4.0	4.8	3.8
W^+W^+	2.8	1.8	2.2	2.0	1.0	0.50	0.50	1.0

W^+W^+ channel for the SM.

Of course, in the case of the W^+W^+ and W^+Z channels we may also add in the negative-charge modes. Because of the fact that the down-quark distribution function is smaller than that for the up quark at moderate-to-large x (high invariant masses probe fairly sizable x values), these event rates are always smaller than those of the positive charge channels. One finds that the W^-W^- signal event rate is about $\frac{1}{3}$ to $\frac{1}{2}$ of the W^+W^+ rate. Similarly, the ratio of W^-Z to W^+Z signal event rates is about $\frac{1}{2}$ to $\frac{2}{3}$ for the models considered here. Meanwhile, the irreducible $TT+LT$ background rates decrease by about a factor of $\frac{2}{3}$ in both channels. By combining the channels of both charges, the observability of the $W^+W^+ + W^-W^-$ and $W^+Z + W^-Z$ signals is somewhat enhanced over the results given in the tables. It is important to note that one of the best means for checking that we are observing the signal of interest is to measure the ratio of W^+W^+ to W^-W^- and W^+Z to W^-Z, respectively. Should the ability of the detectors to discriminate between lepton charges at high momentum be inadequate, we would expect these ratios to be near unity.

In obtaining our LHC results, we have used cuts (as detailed in Sec. II) that are closely analogous to those employed for the SSC. In so doing, we did not attempt to optimize the cuts to the same extent as we did for the SSC. Thus it is possible that the signal/background ratios could be improved, although we do not anticipate that further optimization would lead to any dramatic changes. From Tables VII(a) and VII(b) we see that in the W^+Z, ZZ, and W^+W^+ channels the LHC with a 100 fb^{-1} luminosity is roughly equivalent to the SSC with 10 fb^{-1}, except for the vector models. Because of the large resonance masses, the vector models are more difficult to see at the LHC than at the SSC. In the W^+W^- channel, the SSC has a distinct advantage over the LHC for all models. This is due to the relatively

greater difficulty in removing the $t\bar{t}$ background at the LHC. Another issue of concern for the LHC is the large probability of having multiple interactions in one crossing, yielding many minimum-bias and minijet events superimposed on each WW event of interest. This type of pileup is likely to significantly increase the background levels beyond those computed here on the basis of one collision per crossing. In addition, isolation criteria, the central jet veto, and jet tagging, all of which are central to our analysis, could become much more difficult to implement. In this case, detection of strong interactions in the various W_LW_L channels would be substantially more difficult at the LHC than at the SSC.

V. DISCUSSION

An important question is the extent to which we have truly optimized the procedures for isolating an LL signal in the various WW purely leptonic final-state channels. Below we discuss several improvements that might turn out to be feasible.

A possible improvement in the significance of the signals in the W^+W^- and W^+W^+ channels can be obtained by tightening the cut on $\cos\phi_{ll}$. The improvement that can be obtained, based on our EWA/ET parton-level Monte Carlo program, is illustrated in Table VIII in the case of the W^+W^- channel. By tightening the cut from $\cos\phi_{ll} < -0.8$ to $\cos\phi_{ll} < -0.96$, the background is reduced to $\frac{3}{4}$ of its previous size, while the LL signal rate is decreased by at most 4% (in the SM and scalar cases) and, perhaps, by as little as 2% (vector and CG LET models). Such a large decrease in the background level would clearly lead to an increase in the significance of the signals in these channels.

However, these results were obtained using the EWA/ET calculation in which the transverse momentum of the W_LW_L pair, $p_T(WW)$, is ignored. A nonzero

TABLE VIII. Percentage decrease in the SSC event rate for the W^+W^- channel relative to the $\cos\phi_{ll} < -0.8$ cut results presented in Table V(a).

W^+W^-	Bkgd.	SM	Scalar	O(2N)	Vec. 2.0	Vec. 2.5	CG LET	K LET	K delay
$\cos\phi_{ll} < -0.96$	25	3.7	4.3	3.5	2.3	2.3	2.0	2.2	2.2

value for $p_T(WW)$ would imply that the $W_L W_L$ are not exactly back to back. Previously, we noted the $1/(p_T^2 + M_W^2)^2$ distribution of the W_L's which initiate the $W_L W_L$ scattering (as measured with respect to the quarks from which they are emitted). This steep falloff implies that $p_T(WW)$ for the $W_L W_L$ signal is very limited (in contrast to the $W_L W_T$ and $W_T W_T$ background). Typically, $p_T(WW)$ for the $W_L W_L$ scattering signal is not much larger than M_W. For an event with $p_T(W) \sim 0.5$ TeV, $p_T(WW) \sim M_W$ can result in angle of $\phi \approx 162°$ [for the configuration where $p_T(WW)$ is perpendicular to the individual p_T's of the Ws], which corresponds to $\cos\phi(WW) \approx -0.95$. Thus, although the agreement between the exact "subtraction" calculation and the EWA/ET calculation is excellent for a modest cut at -0.8, as illustrated by the $W^+ W^+$ comparison of Table IV, this agreement might worsen if the cut is strengthened. Indeed, in the $W^+ W^-$ channel we have found that the exact "subtraction" results with $\cos\phi_{ll} < -0.96$ is about 77% as much as that with $\cos\phi_{ll} < -0.8$, as compared to the 4% decrease listed in Table VIII obtained using the EWA/ET amplitudes. Further, there are additional sources of $p_T(WW)$. A Monte Carlo program which goes beyond the parton level will include initial-state radiation of gluons, the intrinsic transverse momentum of the quarks that initially radiate the fusing Ws, and hard gluon radiation in the final state (part of the higher-order QCD corrections to the $W_L W_L$ scattering process). All of these effects will tend to impart some net transverse momentum to the $W_L W_L$ pair and decrease the fraction of lepton pairs that are sufficiently back to back to pass a very severe cut on $\cos\phi_{ll}$. We anticipate that the -0.8 cut is sufficiently moderate that such effects will not significantly alter the efficiencies obtained from a parton Monte Carlo program. It is worthwhile to notice that the effects of $p_T(WW)$ are less important for models with more events in the larger mass region $[M(WW) > 1$ TeV], such as the CG LET. This was also demonstrated in Ref. [31], where an empirical formula for the $p_T(WW)$ spectrum was used in combination with the EWA.

Regardless of which $\cos\phi_{ll}$ cut turns out to be most appropriate, one can ask whether it would be beneficial in the ZZ and WZ channels. We have not imposed this cut in our work because background event rates in these channels are already small after the cuts employed, and the amount of improvement in the significance of a signal would be marginal. It is only if some of the cuts that we have employed must be significantly weakened or if our cuts are not so efficient in eliminating the background, when the actual data is analyzed, that a $\cos\phi_{ll}$ cut in these channels might prove valuable.

Another issue is the extent to which our cuts eliminate a contribution to the LL signals of interest arising from a source quite distinct from the $W_L W_L$ scattering processes upon which we have focused. An example of such a situation arises in the case of the WZ channel. If the appropriate model contains a spin-one-isospin-one resonance, then a larger signal rate is obtained by eliminating the jet-tag cut. This is because there is an additional con-

tribution from $q\bar{q}$ fusion in which a virtual W is created that then mixes with the vector resonance. Some analysis of this situation has appeared in Refs. [42,51,52], where it was found that one might be able to observe a signal without jet tagging if such a resonance exists. However, eliminating the jet tagging is much more likely to be viable at the SSC than at the LHC. In Tables II(a) and II(b), we saw that the signal/background ratio becomes much worse at the LHC than at the SSC if jet tagging is not performed. Clearly, a careful study is required; this is beyond the scope of the present paper.

We must not forget that, for each channel, we have considered only the "gold-plated" purely leptonic decay modes containing the maximum possible number of charged leptons. These are the cleanest modes for observing the LL signal, but a significant price is paid in terms of branching ratios. The next cleanest mode that can be considered is $ZZ \rightarrow l^+ l^- \nu\bar{\nu}$. This mode has roughly 6 times as large a branching ratio as the four-charged-lepton mode we have studied. Parton-level calculations [53] and some recent SDC detector studies [29] indicate that cuts can be implemented which could eliminate reducible backgrounds in this mode. The only issue is the extent to which the irreducible EW $Z_T Z_T + Z_T Z_L$ backgrounds can be suppressed. Some study of this has appeared in Ref. [51]. There, it is found that a significant improvement in the observability of the $Z_L Z_L$ signal can be obtained for several models if the $l^+ l^- \nu\bar{\nu}$ mode is employed.

Of course, WW final states containing a mixture of leptons and jets have still higher branching ratios. However, mixed QCD-electroweak backgrounds enter. Many of the techniques that we have developed here for isolating the purely leptonic signals will also be applicable for such mixed states, and additional cuts will become relevant, e.g., a cut on multiplicity and/or rapidity structure [54,55]. A refined study of the mixed modes, incorporating some of the procedures that have been developed for the purely leptonic modes, should be performed [6], but is beyond the scope of this paper.

We have demonstrated the importance of using the single jet tagging to enhance the signal/background ratio, especially for the $W^+ W^-$ mode to suppress the huge $t\bar{t}$ background [14].

Our resulting tagging efficiency for the signal agrees well with the full Monte Carlo study for the SDC detector [29]. This is also true for the background process $t\bar{t}j$;[2] our fixed order-α_s^3 parton-level calculation agrees quite well with results quoted in the SDC report [29]. Nonetheless, still more careful studies of jet tagging in the forward/backward region would be worthwhile.

VI. CONCLUSIONS

We have demonstrated that, at both the SSC and LHC, viable signals for strong $W_L W_L$ interactions can be ob-

---

[2]In preliminary versions of this work, a programming error led to an apparent disagreement [14].

tained for a wide variety of models in the purely leptonic final states. Of course, the channels examined, $W^+W^- \rightarrow l^+l^-\nu\bar{\nu}$, $W^+Z \rightarrow l^+l^-l\nu$, $ZZ \rightarrow l^+l^-l^+l^-$, and $W^+W^+ \rightarrow l^+l^+\nu\nu$, do not *all* yield adequate signals in 1–2 years of canonical SSC or LHC luminosity for *all* models. Instead, we find that a significant signal can always be found in the channels that most naturally complement the particular type of model considered. In particular, models with a resonance of definite isospin are most easily probed using the WW channels that have resonant contributions from that same isospin. Indeed, one of our more important conclusions is that different types of models can be distinguished experimentally by determining the relative magnitude of the LL signals in the four channels listed above.

A large part of our work focused on the techniques required to suppress reducible and, especially, irreducible backgrounds to a level such that the low LL signal event rates in the purely leptonic channels can be isolated. In particular, the irreducible backgrounds from production of WW pairs with TT and LT polarizations end up being most important, and our techniques are particularly focused on suppressing them. Although our calculations do not include detector effects, we believe that they will survive more sophisticated Monte Carlo analyses. In particular, the types of cuts we have employed should be directly applicable in the experimental analyses that will be performed when actual data become available.

Overall, we conclude that it is possible to probe a strongly interacting electroweak symmetry-breaking sector at the SSC or LHC using only the "gold-plated" purely leptonic modes studied here. Even if a light Higgs boson is found, it will be important to measure the event rates at high $M(WW)$ in all the various channels in order

to make certain that the Higgs boson completely cures the bad high-energy behavior in all WW scattering subprocesses. The low event rates for the purely leptonic final states imply that of order 2–3 years of 10 fb^{-1} annual luminosity will be required to conclude that there is no obvious $W_L W_l$ enhancement in any of the four channels. Because of the relative cleanliness of these final states, the option of achieving this required integrated luminosity via enhanced instantaneous luminosity should be strongly considered.

[1] D. A. Dicus and V. S. Mathur, Phys. Rev. D **7**, 3111 (1973); B. W. Lee, C. Quigg, and H. Thacker, *ibid.* **16**, 1519 (1977); M. Veltman, Acta Phys. Pol. B **8**, 475 (1977).

[2] M. S. Chanowitz and M. K. Gaillard, Nucl. Phys. **B261**, 379 (1985).

[3] J. M. Cornwall, D. N. Levin, and G. Tiktopoulos, Phys. Rev. D **10**, 1145 (1974); C. Vayonakis, Lett. Nuovo Cimento **17**, 383 (1976); G. J. Gounaris, R. Kogerler, and H. Neufeld, Phys. Rev. D **34**, 3257 (1986); Y.-P. Yao and C.-P. Yuan, *ibid.* **38**, 2237 (1988); J. Bagger and C. R. Schmidt, *ibid.* **41**, 264 (1990); H. Veltman, *ibid.* **41**, 2294 (1990); H.-J. He, Y.-P. Kuang, and Xiaoyuan Li, Phys. Rev. Lett. **69**, 2619 (1992).

[4] M. S. Chanowitz and M. K. Gaillard, Phys. Lett. **142B**, 85 (1984); G. L. Kane, W. W. Repko, and W. R. Rolnick, *ibid.* **148B**, 367 (1984); S. Dawson, Nucl. Phys. **B249**, 42 (1985).

[5] J. Lindfors, Z. Phys. C **28**, 427 (1985); J. F. Gunion, J. Kalinowski, and A. Tofighi-Niaki, Phys. Rev. Lett. **57**, 2351 (1986); W. B. Rolnick, Nucl. Phys. **B274**, 171 (1986); P. W. Johnson, F. I. Olness, and Wu-Ki Tung, Phys. Rev. D **36**, 291 (1987); Z. Kunszt and D. E. Soper, Nucl. Phys. **B296**, 253 (1988); A. Abasabadi, W. W. Repko, D. A. Dicus, and R. Vega, Phys. Rev. D **38**, 2770 (1988); S. Dawson, Phys. Lett. B **217**, 347 (1989).

[6] For a review, see C.-P. Yuan, in *Perspectives On Higgs Physics*, edited by Gordon L. Kane (World Scientific, Singapore, 1993).

[7] R. Dashen and H. Neuberger, Phys. Rev. Lett. **50**, 1897 (1983); J. Kuti, L. Lin, and Y. Shen, *ibid.* **61**, 678 (1988); M. Luscher and P. Weisz, Phys. Lett. B **212**, 472 (1988); Nucl. Phys. **B318**, 705 (1989); U. M. Heller *et al.*, *ibid.* **B405**, 555 (1993).

[8] Gunion, Kalinowski, and Tofighi-Niaski [5].

[9] R. N. Cahn *et al.*, Phys. Rev. D **35**, 1626 (1987); V. Barger, T. Han, and R. J. N. Phillips, *ibid.* **37**, 2005 (1988); R. Kleiss and W. J. Stirling, Phys. Lett. B **200**, 193 (1988).

[10] D. Froideveaux, in *Proceedings of the ECFA Large Hadron Collider Workshop*, Aachen, Germany, 1990, edited by G. Jarlskog and D. Rein (CERN Report No. 90-10, Geneva, Switzerland, 1990), Vol. II, p. 444; M. H. Seymour, *ibid.*, p. 557.

[11] U. Baur and E. W. N. Glover, Nucl. Phys. **B347**, 12 (1990); Phys. Lett. B **252**, 683 (1990).

[12] V. Barger, K. Cheung, T. Han, and R. J. N. Phillips, Phys. Rev. D **42**, 3052 (1990).

[13] V. Barger, K. Cheung, T. Han, J. Ohnemus, and D. Zeppenfeld, Phys. Rev. D **44**, 1426 (1991).

[14] V. Barger, K. Cheung, T. Han, and D. Zeppenfeld, Phys. Rev. D **44**, 2701 (1991); **48**, 5444E (1993); **48**, 5433 (1993).

[15] V. Barger, K. Cheung, T. Han, A. Stange, and D. Zeppenfeld, Phys. Rev. D **46**, 2028 (1992).

[16] D. Dicus, J. F. Gunion, and R. Vega, Phys. Lett. B **258**, 475 (1991).

[17] D. Dicus, J. F. Gunion, L. H. Orr, and R. Vega, Nucl. Phys. **B377**, 31 (1991).

[18] Talks given by W. Smith, F. Paige, and T. Han, presented at the SSC Physics Symposium, Madison, Wisconsin, 1991 (unpublished).

[19] R. W. Brown and K. O. Mikaelian, Phys. Rev. D **19**, 922 (1979).

[20] U. Baur, E. W. N. Glover, and J. J. van der Bij, Nucl. Phys. **B318**, 106 (1989); V. Barger, T. Han, J. Ohnemus, and D. Zeppenfeld, Phys. Rev. D **41**, 2782 (1990).

[21] J. Ohnemus and J. F. Owens, Phys. Rev. D **43**, 3626 (1991); B. Mele, P. Nason, and G. Ridolfi, Nucl. Phys. **B357**, 409 (1991).

[22] D. A. Dicus, C. Kao, and W. W. Repko, Phys. Rev. D **36**, 1570 (1987); E. W. N. Glover and J. J. van der Bij, Nucl. Phys. **B321**, 561 (1989).

[23] D. A. Dicus, S. L. Wilson, and R. Vega, Phys. Lett. B **192**, 231 (1987).

[24] V. Barger, T. Han, and R. J. N. Phillips, Phys. Lett. B **200**, 193 (1988); U. Baur and E. W. N. Glover, Phys. Rev. D **44**, 99 (1991).

[25] R. K. Ellis and J. C. Sexton, Nucl. Phys. **B282**, 642 (1987).

[26] P. Nason, S. Dawson, and R. K. Ellis, Nucl. Phys. **B303**, 607 (1988); W. Beenakker *et al.*, Phys. Rev. D **40**, 54 (1989); Nucl. Phys. **B351**, 507 (1991).

[27] R. Kleiss and W. J. Stirling, Z. Phys. C **40**, 419 (1988); H. Baer, V. Barger, and R. J. N. Phillips, Phys. Rev. D **39**, 2809 (1989); H. Baer, V. Barger, J. Ohnemus, and R. J. N. Phillips, *ibid.* **42**, 54 (1990); R. P. Kauffman and C. P. Yuan, *ibid.* **42**, 956 (1990); G. A. Ladinsky and C. P. Yuan, *ibid.* **43**, 789 (1990).

[28] V. Barger, A. D. Martin, and R. J. N. Phillips, Phys. Lett. **125B**, 339 (1983); V. Barger, T. Han, and J. Ohnemus, Phys. Rev. D **37**, 1174 (1988).

[29] SDC Technical Design Report No. SDC-92-201, 1992 (unpublished).

[30] M. S. Chanowtiz and M. Golden, Phys. Rev. Lett. **61**, 1053 (1988); **63**, 466(E) (1989).

[31] M. S. Berger and M. S. Chanowitz, Phys. Lett. B **263**, 509 (1991).

[32] D. A. Dicus and R. Vega, Phys. Lett. B **217**, 194 (1989).

[33] For a review, see, e.g., J. Bagger, in *Perspectives in the Standard Model*, Proceedings of the 1991 Theoretical Advanced Study Institute, Boulder, Colorado, edited by R. K. Ellis, C. T. Hill, and J. D. Lykken (World Scientific, Singapore, 1992).

[34] C.-P. Yuan, Nucl. Phys. **B310**, 1 (1988).

[35] G. L. Kane and C.-P. Yuan, Phys. Rev. D **40**, 2231 (1989).

[36] S. Willenbrock and G. Valencia, Phys. Lett. B **247**, 341 (1990); Phys. Rev. D **46**, 2247 (1992).

[37] M. Einhorn, Nucl. Phys. **B246**, 75 (1984).

[38] S. Nachulich and C.-P. Yuan, Phys. Lett. B **293**, 395 (1992).

[39] S. Weinberg, Phys. Rev. **166**, 1568 (1968); S. Coleman, J. Wess, and B. Zumino, *ibid.* **177**, 2239 (1969); C. Callan, S. Coleman, J. Wess, and B. Zumino *ibid.* **177**, 2247 (1969); S. Weinberg, Physica **96A**, 327 (1979).

[40] S. Weinberg, Phys. Rev. Lett. **17**, 616 (1966); M. S. Chanowitz, M. Golden, and H. Georgi, *ibid.* **57**, 2344 (1986); Phys. Rev. D **35**, 1490 (1987).

[41] R. Casalbuoni *et al.*, Phys. Lett. **155B**, 95 (1985); Nucl. Phys. **B282**, 235 (1987); see also M. Bando, T. Kugo, and K. Yamawaki, Phys. Rep. **164**, 217 (1988), and references therein.

[42] R. Casalbuoni *et al.*, Phys. Lett. B **249**, 130 (1990); **253**, 275 (1991); J. Bagger, T. Han, and R. Rosenfeld, in *Research Directions for the Decade*, Proceedings of the Summer Study, Snowmass, Colorado, 1990, edited by E. Berger (World Scientific, Singapore, 1992).

[43] R. Casalbuoni *et al.*, Phys. Lett. B **269**, 361 (1991).

[44] A. Dobado, M. Herrero, and J. Terron, Z. Phys. C **50**, 205 (1991); **50**, 465 (1991); S. Dawson and G. Valencia, Nucl. Phys. **B348**, 23 (1991); **B352**, 27 (1991); Bagger, Dawson, and Valencia, in *Research Directions for the Decade* [42].

[45] J. Gasser and H. Leutwyler, Ann. Phys. **158**, 142 (1984); Nucl. Phys. **B250**, 465 (1985); J. Bagger, S. Dawson, and G. Valencia, *ibid.* **B399**, 364 (1993).

[46] See, however, A. F. Falk, M. Luke, and E. H. Simmons, Nucl. Phys. **B365**, 523 (1991).

[47] J. G. Morfin and W.-K. Tung, Z. Phys. C **52**, 13 (1991).

[48] M. Berger and M. Chanowitz, Phys. Lett. B **267**, 416 (1991).

[49] T. Han, G. Valencia, and S. Willenbrock, Phys. Rev. Lett. **69**, 3274 (1992).

[50] J. F. Gunion, J. Kalinowski, A. Tofighi-Niaki, A. Abbasabadi, and W. Repko, in *Physics of the Superconducting Supercollider, Snowmass, 1986*, Proceedings of the Summer Study, Snowmass, Colorado, edited by R. Donaldson and J. Marx (Division of Particles and Fields of the APS, New York, 1987); Gunion *et al.* [5]; Abbasabadi *et al.* [5].

[51] M. Chanowitz, in *Proceedings of the XXVth International Conference on High Energy Physics*, Dallas, Texas, 1992, edited by J. R. Sanford, AIP Conf. Proc. No. 272 (AIP, New York, 1993); presented at the Workshop on Electroweak Symmetry Breaking at Colliding-Beam Facilities, Santa Cruz, California, 1992 (unpublished).

[52] A. Dobado, M. J. Herrero, and T. N. Truong, Phys. Lett. B **235**, 129 (1990).

[53] R. N. Cahn and M. Chanowitz, Phys. Rev. Lett. **56**, 1327 (1986); V. Berger, T. Han, and R. Phillips, Phys. Rev. D **36**, 295 (1987).

[54] J. F. Gunion *et al.*, Phys. Rev. D **40**, 2223 (1989).

[55] J. D. Bjorken, Phys. Rev. D **47**, 101 (1993); in *Photon-Photon '92*, Proceedings of the IXth Workshop on Photon-Photon Collisions, San Diego, California, 1992, edited by D. O. Caldwell and H. P. Paar (World Scientific, Singapore, 1992).
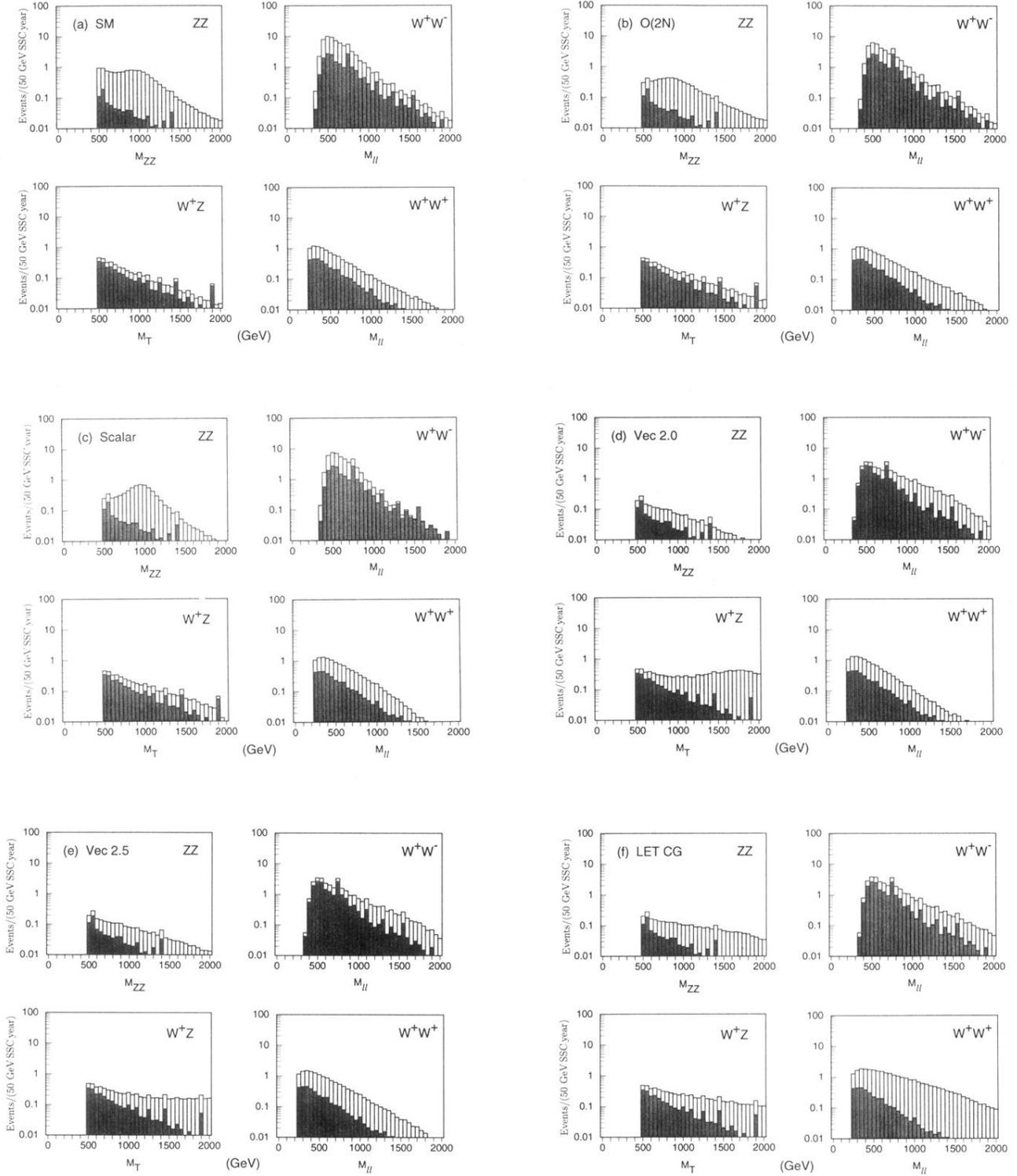
FIG. 3. Invariant mass distributions for the "gold-plated" leptonic final states that arise from the processes $pp \rightarrow ZZX$, $pp \rightarrow W^+W^-X$, $pp \rightarrow W^+ZX$, and $pp \rightarrow W^+W^+X$, for $\sqrt{s} = 40$ TeV and an annual SSC luminosity of 10 fb^{-1}. The longitudinally polarized signal is plotted above the summed background. The mass variable of the x axis is in units of GeV, and the bin size is 50 GeV. (a) SM with a 1-TeV Higgs boson; (b) O(4) model with $\Lambda = 3$ TeV; (c) chirally coupled scalar with $M_S = 1$ TeV, $\Gamma_S = 350$ GeV; (d) chirally coupled vector with $M_V = 2$ TeV, $\Gamma_V = 700$ GeV; (e) chirally coupled vector with $M_V = 2.5$ TeV, $\Gamma_V = 1300$ GeV; (f) nonresonant model unitarized following Chanowitz and Gaillard; (g) nonresonant model unitarized by the K-matrix prescription; (h) $O(p^4)$ nonresonant model with delayed unitarity violation, unitarized by the K-matrix prescription.
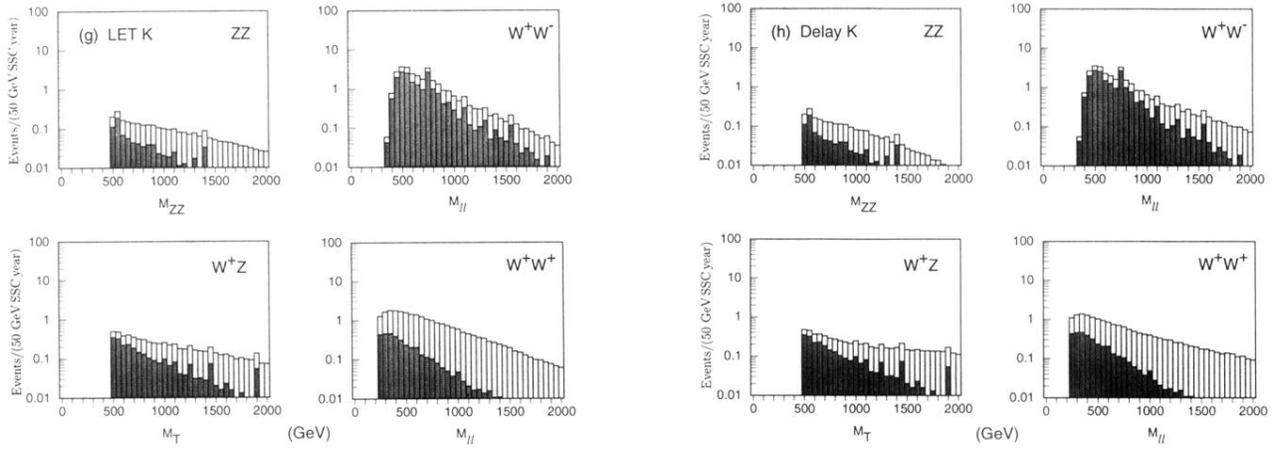
FIG. 3. (*Continued*).